Research Square

Preprints are preliminary reports that have not undergone peer review.
They should not be considered conclusive, used to inform clinical practice,
or referenced by the media as validated information.

Impact of UAV Flight Parameters and Acquisition Context for Canopy Height and Trunk Circumference Measurement Using LiDAR

Clément Battista

clement.battista@inrae.fr

ISPA, UMR1391 INRAE/Bordeaux Science Agro

Frédéric Frappart

ISPA, UMR1391 INRAE/Bordeaux Science Agro

Martin Schwartz

CEA, CNRS, UVSQ, Université Paris-Saclay

Frédéric Baup

Université de Toulouse, CNES/CNRS/INRAE, IRD/UT3

Research Article

Keywords: UAV LiDAR, tree-level metrics, canopy height, trunk circumference, flight configuration, plantation forestry

Posted Date: April 26th, 2026

DOI: https://doi.org/10.21203/rs.3.rs-9310794/v1

License: This work is licensed under a Creative Commons Attribution 4.0 International License.
Read Full License

Additional Declarations: No competing interests reported.

Abstract

UAV-borne LiDAR has emerged as a promising tool for tree-level forest inventory, yet the influence of flight parameters and acquisition context on the accuracy of structural metrics remains insufficiently documented. This study evaluates how UAV flight altitude, speed, area margins, number of returns, flight plan geometry, and seasonal conditions affect the estimation of canopy height and trunk circumference in a managed 0.23-ha poplar plantation in southwestern France. Twenty-two UAV flights were conducted between 2024 and 2025 using a DJI Matrice 300 equipped with a Zenmuse L1 LiDAR sensor, with systematically varied acquisition parameters. Tree-level metrics derived from point clouds were compared with field measurements, terrestrial LiDAR scans, airborne LiDAR (IGN LiDAR HD), and satellite-derived canopy height maps (FORMS-T).

Canopy height estimation proved highly robust across UAV flights, showing close agreement with terrestrial LiDAR (R^2 = 0.99, RMSE = 0.33 m) and consistency with expected poplar growth rates (0.9–1.4 $m \cdot yr^{-1}$). Reliable height retrieval required a minimum point density of approximately 1,000 $pts \cdot m^{-2}$, and flight altitudes below about 60 m above the canopy. In contrast, trunk circumference estimation was more sensitive to acquisition parameters and environmental conditions. Accurate retrieval was achieved only under leaf-off conditions, with optimal performance obtained using low flight altitudes (≤ 80 m), triple-return acquisition, high margins, and flight paths aligned with plantation rows (R^2 = 0.76–0.90; RMSE = 12–35 cm, or 4–11 cm for DBH). Leaf-on acquisitions and understory regrowth substantially reduced accuracy. This study provides practical guidelines for optimizing UAV flight planning in plantation forests and improves the reproducibility of UAV-based forest structural monitoring.

1. Introduction

Accurate characterization of forest structure is fundamental for estimating above-ground biomass (Vashum et al., 2012; Kumar et al., 2017), monitoring forest dynamics, and informing sustainable management and carbon accounting (Houghton, 2005; Temesgen et al., 2015). Structural attributes such as Diameter at Breast Height (DBH) and tree height are central variables in allometric models linking field measurements to biomass and volume estimates (Muukonen, 2007). These parameters are traditionally obtained through in situ forest inventories, divided into two types: remote methods and contact-measurements methods, using manual instruments such as measuring tapes, calipers and tree girders (Binot et al., 1995; West, 2009), and hypsometers (Bragg, 2014) or optical dendrometers (Grosenbaugh, 1963; Keeland et al., 1993). While these methods remain the standard for field-based forest assessments, they are time-consuming, labor-intensive, and limited in spatial coverage, particularly in heterogeneous or inaccessible environments.

In France, poplars (Populus spp.) are widely cultivated in alluvial valleys and wet lowlands due to their rapid growth, homogeneous wood quality, and ease of regeneration. They are primarily grown for industrial uses, including veneer, packaging, and pulpwood production (IGN, 2022). Management typically involves short rotations of 20–25 years and regular silvicultural interventions such as clearing,

pruning, and thinning (Dickmann & Stuart, 1983). At the national level, poplar cultivation is supported by breeding programs and regional development plans aimed at improving productivity, disease resistance (particularly against rust) and site adaptation (FCBA, 2018). Because of their uniform structure, spacing, and fast growth, poplar plantations provide an ideal framework for developing and testing high-resolution remote sensing techniques dedicated to tree-level structural analysis (Mapuru et al., 2023).

Over the past two decades, LiDAR (Light Detection and Ranging) technology has become a reference tool for quantifying forest structure in three dimensions, and estimating above ground biomass (Zolkos et al., 2013). LiDAR systems produce dense point clouds describing canopy and trunk geometry and have been deployed from various platforms ranging from terrestrial to airborne and satellite systems (Lu et al., 2016). Terrestrial Laser Scanners (TLS) deliver millimetric accuracy and are widely used for tree-level characterization (Calders et al., 2022), but their operation requires multiple static scans per plot and substantial field time. Backpack-mounted LiDAR systems were initially developed for urban mapping (Puente et al., 2013; Zolanvari et al., 2019) but have since demonstrated their utility in forestry applications (Hopkinson et al., 2004; Huang et al., 2011; Brede et al., 2017; Liu et al., 2018; Xie et al., 2022; Hui et al., 2024). Compared with static TLS systems, backpack-mounted sensors allow faster and continuous data acquisition, though they typically produce lower local point densities and slightly reduced positional accuracy due to operator movement. Nevertheless, they can be difficult to operate in dense understory conditions when the forest floor is covered by low trees or other vegetation.

Airborne LiDAR (ALS) enables efficient large-area coverage, but individual-tree analysis often requires sufficiently high point density and remains challenged by occlusion and reduced detail in lower canopy layers (Eysn et al., 2015; Hamraz et al., 2017). The recent emergence of Unmanned Aerial Vehicle (UAV)-borne LiDAR systems bridges this gap, combining flexible acquisition geometry with high spatial resolution (Ferraz et al., 2016). UAV platforms enable low-altitude data acquisition with customizable flight parameters, providing a unique opportunity to optimize LiDAR performance for specific forest structures (Eisenschink et al., 2025). However, the accuracy of LiDAR-derived metrics depends strongly on acquisition conditions such as flight altitude, scan angle, point density, and the number of recorded returns. Despite rapid technological advances, the quantitative impact of these parameters on the estimation of key forest attributes, particularly tree height and trunk circumference, remains insufficiently characterized.

The objective of this study is to quantify the impact of UAV flight parameters on the accuracy of canopy height and trunk circumference measurements obtained from UAV LiDAR data. By analyzing the combined effects of acquisition geometry, point density, return configuration, and vegetation phenology, this work seeks to identify optimal acquisition conditions for UAV-based forest inventories in plantation environments. Beyond the specific case of poplar stands, the findings contribute to improving the reproducibility and operational value of UAV LiDAR methods for structural forest monitoring.

To this end, the manuscript is structured as follow: the Materials and Methods section presents the study site, the LiDAR datasets (UAV LiDAR, TLS, ALS) and satellite products, as well as the point-cloud

processing workflow used to extract canopy height and trunk circumference. The Results section then reports the accuracy of the retrieved structural metrics under the different flight configurations and acquisition contexts. The Discussion section examines the influence of key parameters (e.g., flight altitude, point density, return mode, flight plan geometry, and seasonality) and derives practical recommendations for UAV LiDAR acquisition planning in plantation forests. Finally, the Conclusion summarizes the main findings and highlights perspectives for operational applications and future work.

2. Material

2.1. Study Area

The study site (3.690893° N, 0.464305° E) is located in southwestern France, within the Occitanie region, in the town of Ordan-Larroque, (Fig. 1a–e). The area is governed by a temperate oceanic climate, with an average annual precipitation of approximately 847 mm and a mean temperature of 13.4°C, calculated over the 2022–2025 period based on climatic data from the weather station located in the city of Auch and freely available on climate-data.org.. The site lies within a 1.4 ha poplar (*Populus* spp.) plantation, bordered by monoculture fields and hedges. The plot is traversed by drainage ditches with a small stream running alongside. The specific study area occupies 0.23 ha in the southern portion of the plot. The terrain is nearly flat at an average elevation of 149 m, with a gentle slope (~ 1%) rising toward the southwest.

The surveyed area contains 33 poplar trees (Fig. 1e) within a privately managed plantation of approximately 240 individuals (Fig. 2), planted two decades ago, in 2001.

Within the study area, trees are planted in regular rows, oriented northwest–southeast, with a spacing of 7 m in both directions. Some of them have been removed following storm damage. Underwood vegetation is periodically cleared mechanically to maintain open ground, and trunks are pruned to facilitate plantation management (Fig. 2).

2.2. UAV LiDAR dataset

UAV lidar dataset has been acquired by a Zenmuse L1 LiDAR sensor (DJI), which emits laser pulses at a wavelength of 905 nm, achieving a ranging accuracy of 3 cm at 100 m and a pulse rate of up to 240,000 pts.s^{-1}, with up to three returns per pulse (DJI, 2025). Additionally, 20 MP RGB images were acquired for photogrammetric processing, enabling the production of an orthophoto with a spatial resolution of 1.64 cm.$pixel^{-1}$, at a flight altitude of 60 m above ground level. The sensor was mounted on a Matrice 300 (DJI) UAV equipped with RTK capabilities to ensure high geolocation accuracy (< 5cm in planimetric and vertical directions).

A total of 22 UAV flights were conducted over the study area between January 2024 and April 2025. Flight parameters were systematically modified to assess their impact on data quality, including altitude above ground level, point density (pts.m^{-2}), flight speed and trajectory, overlap between adjacent flight

lines, buffer margins at plot boundaries, number of returns recorded, and sampling strategies. Operations were constrained by the maximum allowable flight altitude of 120 m. A detailed list of flight characteristics is provided in Table 1.

Table 1
Characteristics of UAV LiDAR acquisitions conducted in January 2024, January 2025, and April 2025.

Flight number	Date	Density	GSD	Flight altitude	Speed	Flight angle	Return mode	Data weight
-	-	pt/m²	cm	m	$m.s^{-1}$	° to plantation rows		$Go.Ha^{-1}$
1	Jan. 2024	671	3.27	120	6	0	Dual	0.23
2	Jan. 2024	447	3.27	120	6	0	Triple	0.17
3	Jan. 2024	894	2.46	90	6	0	Dual	0.40
4	Jan. 2024	596	2.46	90	6	0	Triple	0.28
5	Jan. 2024	1519	1.64	60	5.3	0	Dual	1.08
6	Jan. 2024	1013	1.64	60	5.3	0	Triple	0.80
7	Jan. 2024	2025	1.23	45	5.3	0	Dual	1.51
8	Jan. 2024	1350	1.23	45	5.3	0	Triple	1.15
9	Jan. 2024	3838	1.23	45	4	0	Dual	3.10
10	Jan. 2024	1006	2.18	80	6	0	Dual	1.15
11	Jan. 2025	6674	1.23	45	2.3	90	Dual	19.24
12	Jan. 2025	6978	1.23	45	2.2	0	Dual	16.79
13	Jan. 2025	9889	0.96	35	2	90	Dual	5.53
14	Apr. 2025	2683	1.23	45	4	0	Dual	3.85
15	Apr. 2025	3577	1.23	45	3	0	Dual	5.07
16	Apr. 2025	5366	1.23	45	2	0	Dual	7.44

Flight number	Date	Density	GSD	Flight altitude	Speed	Flight angle	Return mode	Data weight
17	Apr. 2025	2683	1.23	45	4	0	Single	1.21
18	Apr. 2025	1789	1.23	45	4	0	Triple	1.46
19	Apr. 2025	4386	1.23	45	3.5	0	Dual	6.67
20	Apr. 2025	12990	1.23	45	1.7	0	Dual	26.79
21	Apr. 2025	2683	1.23	45	4	45	Dual	1.93
22	Apr. 2025	2683	1.23	45	4	90	Dual	1.96

Weather conditions were comparable across all UAV flights (clear skies and low wind speeds), making their influence negligible. However, the timing of data collection varied: 13 UAV flights were conducted in winter when trees were leafless, while 9 flights took place in spring, when trees were largely covered with young foliage.

Raw LiDAR data, acquired in DJI's proprietary format, were converted into .las point clouds using DJI Terra software. The chosen coordinate reference system was Lambert-93 (EPSG:2154), referred to EGM96 as the geoid model.

2.3. Ancillary datasets

2.3.1. In-situ tree heights and circumference at breast height

Three campaigns of *in situ* trunk circumference measurements were conducted in December 2024, April 2025, and October 2025. Measurements were taken using flexible measuring tapes at breast height (1.30 m above ground), following standard DBH (diameter at breast height) protocols (Pretzsch, 2009 ; West, 2015) in December 2024 and April 2025, and at height of 0.60 m, 1.30 m, and 2.00 m in October 2025. These field campaigns, conducted by two different operators and using slightly different measuring tools, yielded highly consistent results (Appendix 1), supporting the reliability of the ground-truth data.

2.3.2. Terrestrial LiDAR Scanner data

Terrestrial LiDAR Scanner (TLS) data were acquired on 23 January 2025, using a portable Viametris MS-96 system (mounted on a backpack) by Parera company.

The system integrates a Velodyne VLP-16 LiDAR sensor, capable of acquiring 320,000–640,000 points.s⁻¹, with a measurement precision of 5 mm (1σ, i.e. one standard deviation) and a range accuracy of ± 1 cm for targets within 120 m. Data geo-referencing is supported by an onboard GNSS receiver and inertial measurement unit (IMU). A connected tablet provides real-time monitoring of satellite connectivity, acquisition trajectory, and point cloud density. Data processing and conversion to .las format were performed using the Viametris software suite.

2.3.3. Airborne Laser Scanning (ALS) LiDAR data

The study site is covered by the national airborne LiDAR survey conducted by the Institut National de l'Information Géographique et Forestière (IGN), specifically as part of the LiDAR HD forest data acquisition program. This survey was conducted using a Leica TerrainMapper sensor, capable of capturing up to 15 returns per pulse (USGS, 2024). Similar to other scientific publications (Daeyeol et al., 2025), IGN chose to retain only five returns. The reported positional accuracies are 5 cm for elevation and 13 cm for horizontal positioning (at 1σ). Each point in the cloud contains additional attributes, including return intensity, echo number, scan angle, and direction (TerrainMapper datasheet). Although LiDAR HD includes an IGN-provided point classification (distinguishing ground, vegetation (low, medium, high), buildings, water surfaces, and other objects) a custom classification was applied in this study to ensure consistency across datasets. Note that these point clouds are distinct from the publicly available IGN digital terrain models (DTMs), as they provide full 3D information including vegetation structure, which is particularly relevant for forest applications.

These data are freely available under the Etalab 2.0 open license via the Géoservices platform (https://geoservices.ign.fr/lidarhd). The dataset (Tiles of 1 km × 1 km) is provided in the Lambert-93 coordinate reference system (EPSG:2154) with the IAG GRS80 ellipsoid. The IGN acquisition over the site was performed on 28 May 2022 (slab 0495–6292), where "slab" refers to the standardized 5 km × 5 km LiDAR tile used by IGN for spatial data organization. The nominal point density for metropolitan France is ≥ 10 pts.m⁻² (excluding high-altitude areas), while the average density over the study site was 36 pts.m⁻².

2.3.4. FORMS-T data

FORMS-T is a national-scale canopy height map (or Digital Height Model, DHM) for France at 10 m spatial resolution, produced every year from 2018 to 2024. It was generated using a deep learning framework combining spaceborne LiDAR from NASA's GEDI (Global Ecosystem Dynamics Investigation) mission with optical and radar data from Sentinel-2 (multispectral) and Sentinel-1 (SAR) missions (Schwartz et al. 2025).

A convolutional neural network (CNN) was trained on GEDI-derived canopy height profiles, serving as reference data, to predict canopy height from Sentinel-2 and Sentinel-1 imagery. The resulting model was applied across the French forest territory to produce the FORMS-T dataset. Vertical accuracy is reported as a mean absolute error (MAE) of ~ 3 m, validated against independent airborne LiDAR datasets and ground-based forest surveys. An overview of the FORMS-T 2024 map used in this study is provided in Fig. 3.

3. Methods

The approach proposed in this study is composed of three main steps: (i) pre-processing to segment individual trees and assign relative point heights (Section 3.1), (ii) extraction of tree heights (Section 3.2), and (iii) computation of trunk circumferences with 3 different methods (Section 3.3). They are summarized in Fig. 4.

The performances of the results are evaluated thanks to the bias, the coefficient of determination (R^2), the root mean square error (RMSE), p-value, and the relative RMSE (rRMSE), established between the estimates and reference dataset (trunks circumference and height).

3.1. Pre-processing and trunk segmentation

Ground points were classified using a progressive morphological filtering algorithm, which identifies the lowest points within regular grid cells and iteratively extends the ground surface under slope and height constraints to preserve local topographic continuity (Esri, 2024). Given the relatively flat terrain of the study area, no additional normalization of the point cloud was required (Dalla Corte, 2020).

Individual trunks of trees were subsequently segmented using a method focused on trunk-level differentiation. Within the 0.6–2 m slice, trees appeared well isolated, with an average spacing of ~ 7 m between stems. A proximity-based clustering approach was implemented: points within 1.5 m of each other were assigned to the same group and considered as belonging to a single tree/trunk.

Finally, trunk centroids were identified by slicing each tree's point cloud into successive 0.20 m layers within the 0.6–2 m height range. For each slice, a mean circle was fitted, and the median centroid of all slices was retained as the trunk center to minimize the influence of low branches or outliers.

3.2. Tree height estimate

Tree height was determined by identifying, for each tree, the highest slice of the point cloud located directly above its centroid within a 2 m radius. This upper slice corresponds to the vertical extent of the point cloud over the tree. The median height of all points within this slice of 0.20 m width was then computed and retained as the tree's canopy height (Fig. 4, Section 3.2). This approach was applied across different data sources (e.g., UAV LiDAR and HD airborne LiDAR). It reduces the influence of noise, which would be more pronounced if the maximum Z-value (Zmax) of each tree's point cloud was used.

In the literature, several approaches have been proposed to estimate tree height from LiDAR data. Some authors used the local maximum height of the LiDAR points as a proxy for tree height (Saarinen et al., 2017 ; Leite et al., 2020). Some others recommend using Z98 or Z95, corresponding to the 98th or 95th percentile of point heights within the tree's point cloud (Hyppa et al., 2008; Ducanson et al., 2014). However, these approaches are not well suited for cross-comparisons among datasets with highly variable point densities in lower canopy strata, and also variable point cloud qualities and were therefore not used in this study.

3.3. Trunk circumference calculation

Three two-dimensional methods were developed to calculate trunk circumference: Mean Circle Fitting (MCF), Maximal Inscribed Circle Fitting (MaxICF) and Spline Fitting (SF) as illustrated in Fig. 4, 3.3 a, b and c, respectively. A detailed overview of these 3 methods is provided in Appendix 2.

They all share a common framework. Each method was applied to all 0.20 m point cloud's slices between 0.60 m and 2.00 m for each tree. For each method and each tree, the shape (circle, or spline) with the smallest circumference was retained, at specific heights. The mean circumference difference between the lowest and highest cross-sections was assessed using three field measurements acquired at 0.60 m, 1.30 m (DBH), and 2.00 m above ground. Between 0.60 m and DBH, the average circumference difference was 9.1 cm (8.5%), whereas between DBH and 2.00 m it decreased to 3.5 cm (3.2%). In addition, the "smallest circumference" selection method was evaluated; it correctly identified the most appropriate cross-sectional representation (circle or spline) for 81% of the trees. Among the remaining 19%, another 7% showed circumference differences smaller than 5%.

Circle-fitting techniques applied to point clouds, particularly to stem cross-sections, have been extensively documented in the literature (Huang et al., 2011; Heo et al., 2019; Guenther et al., 2024) and remain relatively straightforward to implement. In contrast, spline fitting is more complex; as this method is particularly sensitive to point cloud quality, the previously determined trunk centroid (section 3.1) was used as a reference to clean the point cloud for each slice, before spline fitting. This filtering process, inspired by Hui et al. (2024), clusterized points into valid and outlier categories, retaining only those points belonging to the trunk surface while removing branches, ivy, basal shoots, and signal noise.

Final circumference values for each method, named C_{MCF}, C_{MaxICF}, and C_{SF}, were compared to field-measured trunk circumferences for validation.

4. Results

4.1. Tree Height Estimation Across Multiple Sensors

The results of tree height estimates derived from different techniques between 2022 and 2025 are presented in Fig. 5. In 2022, only the LiDAR HD dataset was available for the study area, providing a mean tree height estimate of 19.40 m for the plot (denoted as H_{LHD}). In 2024 and 2025, UAV-based surveys were conducted using the Zenmuse L1 sensor ($H_{UAV\text{-}L1}$). The 2024 flights yielded variable mean tree height estimates ranging between 20 and 21 m, whereas the 2025 flights produced more stable values, averaging around 21.90 m. These latter estimates are consistent with those obtained from the terrestrial LiDAR survey conducted in 2025 (H_{TLS}). Canopy heights measured in 2025 represent an increase of approximately 0.90 m relative to 2024, and 2.50 m relative to 2022, aligning with the lower end of the theoretical annual height increment of poplar trees (0.90–1.40 m; Dickmann & Stuart, 1983).

No significant differences were observed between January and April 2025, which is consistent with the poplar's dormancy period extending into spring.

In 2024, all UAV flights were conducted during the same leaf-off period and revealed lower estimated tree heights when point cloud density was below 1,000 pts.m^{-2} and flight altitude higher than 90 m. Specifically, Flights 1 and 2, with densities of 671 and 447 pts/m², yielded mean heights of approximately 20 m; Flights 3 and 4 (894 and 596 pts/m²), produced slightly higher values around 20.5 m; and Flights 5 to 10, which exceeded 1,000 pts/m², showed mean heights stabilizing around 21 m. The flight altitudes also varied: 120 m for Flights 1 and 2, 90 m for Flights 3 and 4, and between 80 and 45 m for Flights 5 to 10. Flights 1 and 2 exhibited the highest variability, with standard deviations of ~ 3.50 m, compared to ~ 3.30 m (approximately 7% lower variability) for the more stable flights. This suggests a higher sensitivity to data quality and a reduced reliability under lower point densities. In contrast, Flights 5–10 produced consistent and more reliable canopy height estimates.

UAV flights performed in 2025 produced even more homogeneous results, characterized by minimal variation (low standard deviation) and mean H_{UAV-L1} of ~ 21.90 m. The presence or absence of foliage does not appear to have any significant impact on H_{UAV-L1}.

$H_{TLS,}$ collected a few days earlier than the UAV data in 2025, were strongly correlated with these UAV-derived estimates (R^2 = 0.99; RMSE = 0.33 m; rRMSE = 1.50%), further confirming the accuracy and robustness of the methods applied (Appendix 3).

Figure 6 illustrates examples of height comparisons between raster Digital Height Models (DHMs) derived from ALS LiDAR HD data (2022) and UAV LiDAR data (2024), and the corresponding FORMS-T products. In 2022 (Fig. 6.a), the median pixel height over the study area shows a difference of approximately 1.40 m, corresponding to 8.3% relative to the ALS-derived DHM. In 2024 (Fig. 6.b), the median height difference is reduced to approximately 1.87 m (10.1%, when using the UAV-derived DHM as reference). The finer spatial resolution of the ALS- and UAV-derived DHMs (0.5 m, compared to 10 m for FORMS-T) explains their greater sensitivity to within-plot heterogeneity (reflected in higher standard deviations). However, at the scale of the entire stand, particularly in the northern section where the canopy is denser and more tightly packed, these differences tend to diminish (1.6% difference between LiDAR HD and FORMS-T, and 3.7% between UAV LiDAR and FORMS-T).

The mean height growth observed over the study area between 2022 and 2024 based on the different data sources (1.69 m from the ALS- and UAV-derived DHMs, and 1.22 m from FORMS-T) falls within the lower range of expected growth dynamics for poplar stands (Dickmann & Stuart, 1983).

More specifically, when extracting height values from the various datasets along a transect across the plot, the relative hierarchy among tree heights is consistently preserved across all raster products (Fig. 7.a). The underestimation of top heights by FORMS-T, clearly visible in the plot, can be attributed partly to the strongly conical shape of poplar crowns and partly to the use of GEDI RH95 as the training reference for FORMS-T, GEDI RH95 being known to underestimate true canopy tops in stands with

vertical heterogeneity. This effect is likewise evident in models calibrated against airborne LiDAR (ALS) ground truth. The systematic underestimation of tall canopy heights has been widely documented in deep learning-based canopy height estimation studies (Schwartz and al., 2023; Tolan et al., 2024). The Fig. 7.b presents the height growth estimates in two years (2022–2024) calculated on a tree-by-tree basis: it compares the growth results from the original method presented in section 2.2 (point-cloud calculated growth), and the growth results extracted from the DHMs. These results are relatively consistent across datasets, although the point-cloud-based method generally produces higher growth values.

4.2. Tree Trunk Circumference Estimation from Multiple Sensors

Circumference estimation can only be performed on datasets containing trunk-level points. In this study, it corresponds to those acquired with the DJI L1 (UAV) and Viametris MS-96 (terrestrial backpack-mounted) sensors. It was not possible to apply the methods to LIDAR HD data, due to the low point density below the tree's crowns.

Figure 8 summarizes the performance of the UAV flights in estimating trunk circumference using the methods described in section 3.3 (comparison with field-measured tree circumferences). The performance of the three estimation methods is presented: C_{MCF} (a), C_{MaxICF} (b), and C_{SF} (c). For all three methods, flights 1 to 4 yielded poor results, with R^2 values below 0.20. In contrast, flights 5 to 12 produced the most accurate estimates, with R^2 values ranging between 0.50 and 0.90. The remaining flights showed variable performance depending on the method used, but none outperformed flights 5 to 12. For comparison, estimates derived from TLS data consistently showed the highest accuracy (R^2 = 0.96; RMSE = 5.4 cm; bias = − 4.7 cm). The high precision of the ground-based sensor, its proximity to the trunks, and the dense point cloud within a unique slice (averaging ~ 3,800 points per tree in a 6 cm thick slice between 127 cm and 133 cm in height) contribute to these results.

Only flights with a point density exceeding 1,000 pts.m^{-2} successfully accounted for all 33 trees in the plot when applying the smallest spline method. At lower densities, the number of LiDAR returns on stems was insufficient (averaging < 20 points per tree within each slice), and the large RMSE observed highlight substantial variability among trees. The outlier filtering procedure further reduced point counts; since the spline-fitting algorithm requires a minimum of five valid points, many trees were excluded due to data sparsity.

In contrast, the other methods consistently measured all 33 trees, even at lower point densities. However, the resulting estimates exhibited poor accuracy, with R^2 values systematically below 0.2, reflecting the limited reliability of the LiDAR data under these conditions.

The strongest correlations between LiDAR-derived and field-measured circumferences (while retaining all trees) were observed for Flight 9, with R^2 ranging from 0.76 to 0.90 depending on the method. This

flight also featured the highest point density (3838 pts m^{-2}), linked to the highest overlap (80%, against 70% for others comparable flights), enabling precise stem reconstruction within each slice (127 points per tree/slice on average; minimum = 52). Flights 8 and 10 showed similarly strong correlations ($R^2_{Flight\ 8}$ = 0.70–0.83; $R^2_{Flight\ 10}$ = 0.69–0.80), despite a three-fold lower point density.

The smallest RMSE values across all flights (12–14 cm in circumference, equivalent to ~ 4 cm DBH) were achieved by flights 6, 8, and 10.

The three January 2025 flights yielded moderate results, generally inferior to those from the previous year, despite a significant increase in point density per tree, a factor that would be expected to improve performance. The flights conducted in April 2025, in presence of foliage, showed consistent but lower performance compared to flights 11 and 12 carried out in January of the same year. Although none of the methods achieved results comparable to those obtained during the leaf-off period, the SF method yielded the best performance.

Unbiased RMSE (ubRMSE) values decreased: for Flight 9, the RMSE decreased from 20.4–35.6 cm to 9.2–10.2 cm after bias correction (~ 3 cm on DBH). These results are comparable to those reported in the literature; for example, Feng et al. (2022) achieved a lower R^2 (0.71) but a notably lower RMSE (2.1 cm at DBH) using a density of only 110 pts.m^{-2}.

The TLS data presents much better results (R^2=0.96, RMSE = 5.39 cm, rRMSE = 5.22%). It also exhibits a slight underestimation of trunk circumference (bias = -4.69 cm), whereas the UAV data tend to overestimate it (best RMSE: 12.7 cm, for Flight 6 data with SF method). These trends are consistent with the respective characteristics of the two point clouds: the highly accurate TLS point clouds capture well-defined trunk surfaces, which the spline-fitting process slightly simplifies, leading to underestimation; in contrast, the noisier L1 point clouds, combined with the tendency of trunk cross-sections to appear elongated in the flight direction, result in overestimation of circumferences. Methods using circle fitting attenuate the influence of flight planning on the results but fail to compensate for the intrinsic noise of the L1 sensor.

5. Discussion: Impact of Acquisition Parameters

The results presented above provide insights into the relative influence of multiple factors, including both flight parameters and the environmental context in which the UAV operates.

5.1. Flight speed and plan orientation

Several acquisition parameters can affect the margin of error in trunk circumference estimation from UAV LiDAR data. A primary factor is the completeness of the point cloud and its conformity to the expected circular shape (Xie et al., 2022).

In the present study, increasing speed of the flight was found to correlate with an ovalization effect in the point cloud slices, resulting in a systematic elongation along the flight direction. Trunk ovalization is characterized by a Ovalization Ratio approaching 1, as illustrated in Fig. 9a.

Overall, it was observed that as flight speed increases, tree trunks become more ovalized (Ovalization Ratio, OR, tending toward 1), as shown in Fig. 10 and as also suggested by Eisenschink et al. (2025). This ovalization has also been observed in Feng et al., 2022, according to the incidence angle. Inclinations between 55° and 65° have been reported to yield better results than lower angles (which cause significant deformation of trunk geometry) or steeper angles (which provide fewer trunk points in favor of canopy coverage).

In Fig. 9b, the lengths of trunk cross-sections are displayed to allow visual assessment of point cloud orientation and any potential systematic deformation. This effect likely contributes to the overestimation of trunk circumferences and appears unaffected by other flight parameters, except in Flights 1–4, which were otherwise unsuitable for analysis due to poor data quality.

As noted earlier, a flight plan aligned parallel to the axis of the plantation rows appears to be preferable, as it enhances point density around the tree stems. By comparing flights 11 and 12, with similar characteristics but executed with different flight plans (Fig. 9.b), Flight 12 demonstrated the best performance (R^2 = 0.65–0.73; RMSE = 14.1–44.0 cm). Not only is the performance substantially lower for Flight 11, but it is also more heterogeneous across methods (R^2 = 0.28–0.55; RMSE = 39.1–74.4 cm), particularly for the MaxICF method, which is noticeably affected. This effect was also observed during the leaf-on period, between Flight 14 (perpendicular; R^2 = 0.01–0.33) and Flight 21 (parallel; R^2 = 0.08–0.43). This difference is likely attributable to the spatial arrangement of the tree rows: trees are spaced by an average of 7 m apart within rows, but 8 m between rows. Consequently, a flight plan aligned parallel to the rows allows more laser pulses to penetrate the canopy and reach the stems, whereas a perpendicular flight plan results in greater occlusion and reduced stem visibility.

5.2. Number of LiDAR Returns

For tree height estimation, the number of returns recorded by the sensor does not seem to play a major role, as flights capturing three returns yield mean height values (21.02 m) appear very similar to those capturing only two (21.07 m) in the 2024 flights 5 to 10. This is consistent with the density curves shown in Fig. 12, which indicate that no third returns are present within the uppermost 3 m of the tree.

In contrast, the results differ markedly when considering trunk circumference. For instance, Flight 5 (dual-return mode) shows moderate performance (R^2 = 0.46–0.62; RMSE = 17.0–24.8 cm), whereas Flight 6 (triple-return mode) achieves higher and more consistent performance across methods (R^2 = 0.70–0.73; RMSE = 12.4–14.7 cm), despite identical flight parameters. A similar pattern is observed between Flights 7 and 8. Interestingly, this parameter seems to have less influence under leaf-on conditions, as the only flight in April 2025 conducted in triple-return mode (Flight 18) did not outperform the others.

Accounting for the third return of the laser pulse (having passed through upper vegetation strata) enabled better trunk definition. Our analysis indicates that the third return contributes most significantly to point density close to the DBH slice (Fig. 11), being the predominant return between 4.2 m and 1.8 m, as well as at ground level. At DBH height, the third return is comparable to the others. These findings align with Brede et al. (2017), who reported that approximately 60% of trunk points originate from returns beyond the first two.**Figure 11.** *Comparative distribution of LiDAR return density as a function of relative height for a test tree in Flight 7 (dual return mode) and Flight 8 (triple). The inset highlights the 1–6 m slice corresponding to the tree trunk.*

5.3. Flight altitude and margins

Flight altitude, closely linked to point density (lower altitudes yielding denser point clouds), appears to be a key parameter. The first two flights, conducted at the maximum legal altitude of 120 m, failed to adequately capture most tree trunks within the DBH slice and produced canopy height estimates likely underestimated by approximately 1 m. The subsequent flights (Flights 3 and 4), conducted at 90 m, also failed to capture all trunks (26 and 24 out of 33 within the 1.20–1.40 m range) and produced height estimates approximately 50 cm lower than those from Flights 5–10. From an altitude of 80 m (corresponding to ~ 1,000 pts m^{-2}) down to 45 m (i.e., ~ 20–25 m above the canopy), all trunks were clearly defined, and calculated canopy heights were stable and consistent across flights.

For both tree height and trunk circumference, there appears to be no clear relationship between point density and model performance beyond a threshold of approximately 80 m flight altitude and ~ 1,000 pts m^{-2}. Among the 2024 flights, the lowest and densest flight achieved the highest R^2 but also exhibited the highest RMSE, as the point filtering algorithm retained more points, leading to spline fitting on larger, more dispersed clouds. For the 2025 flights, performance generally declined (lower R^2, higher RMSE) with increasing point density. This trend may reflect the algorithm's sensitivity to high point dispersions caused, in part, by surrounding vegetation (see next section).

Closely linked to the flight altitude, another factor that may substantially influence model performance is the extent of the flight margins around the study area. We observed that Flight 10, despite being flown at a relatively high altitude (80 m) with a low point density (1006 pts.m^{-2}) and only two returns, achieved strong performance in trunk circumference estimation (R^2 = 0.69–0.80; RMSE = 13.2–13.7 cm). It successfully captured all trees, unlike Flight 3, which had similar characteristics (90 m altitude, 894 pts m^{-2}, dual return) but much poorer results in trunk circumference estimation (R^2 = 0.01–0.04; RMSE = 32.2–32.4 cm) and in height estimation (0.5 m below flights 5–10 mean height). Flight 5, which featured better acquisition parameters than Flight 10 (60 m altitude, 1519 pts m^{-2}, dual return), also exhibited lower performance (R^2 = 0.46–0.62; RMSE = 17.0–24.8 cm). However, flight plans differed considerably among these acquisitions, which implies that Flight 10 was conducted with broader longitudinal margins around the study plot (Appendix 4). We hypothesize that, although the drone was farther from the plot, additional LiDAR points were still captured over it. This can be explained by the fact that the DJI L1 operates using a *non-repetitive scanning* pattern, in which the sensor's internal mirrors generate a

rotational or quasi-helical scanning trajectory. Even when the camera is oriented in a nadir configuration, as in our study, this mechanism enables the sensor to record points several tens of meters away from the flight line, at oblique viewing angles, very useful for trunk definition. This interpretation is supported by our data: when removing points acquired outside the flight footprints of Flights 3 and 5 from the LiDAR cloud of Flight 10, 43.5% of the points were eliminated (3,455,689 of 7,938,775), leading to a drastic drop in performance in trunk circumference estimation (R^2 = 0.27–0.32). These findings suggest that planning flights with generous margins beyond the study area is advantageous, even if the resulting point cloud must later be cropped to reduce storage requirements. They also indicate that flight altitude can be increased without degrading retrieval performance, while simultaneously reducing acquisition time and point density, provided that sufficiently large margins are maintained around the target area.

5.4. Impact of Seasonality and Silvicultural Management

To estimate the impact of seasonality, two flights with similar characteristics were compared: Flight 11 (January 2025, 6674 pts m^{-2}) and Flight 16 (April 2025, 5366 pts m^{-2}). Across the entire plot, the average number of points per tree within each slice was similar (170 points for Flight 11 vs. 160 for Flight 16). However, the standard deviation was much higher for Flight 16 (123 points, vs. 49 points for Flight 11), reflecting increased variability caused by vegetation growth near tree bases in spring, as observed in the point clouds. When focusing only on trees with “clean” trunks, the difference in normalized point density was 13.3% lower with leaves. Conversely, the uppermost slice of each tree exhibited 46.3% more normalized points in April, indicating that the presence of leaves effectively intercepted laser pulses, preventing them from reaching trunk regions critical for circumference estimation. Given the top-mounted position of the DJI L1 sensor, it is likely that an increased leaf area in spring reduced the proportion of laser pulses reaching lower canopy strata.

Moreover, the presence of understory vegetation substantially influenced circumference determination. This factor is directly linked to silvicultural management in the plot. Between 2024 and 2025, basal regrowth developed around many trunks, generating additional points in the lower canopy and complicating filtering when using DJI L1 data. This made it difficult to distinguish points belonging to tree trunks from those of surrounding vegetation (Fig. 12.a.1), particularly in April 2025, when increased vegetation growth (purple points) is observed compared with January 2024, which is characterized by reduced vegetation cover (light blue points). In contrast, TLS LiDAR (Fig. 12.a.2) was unaffected due to its higher point density at trunk level, enabling efficient discrimination of non-trunk features. Three example trees from the plot, surrounded by low-lying vegetation around the trunk, are shown in Fig. 12.b.

The method selecting the smallest shape (circle or spline) for each stem is designed to mitigate the variable impact of surrounding vegetation and low branches. By adapting to each individual tree, it assumes that the more spatially constrained the point cloud, the closer it lies to the actual trunk surface.

6. Conclusion

This study leveraged LiDAR data acquired with the DJI L1 sensor during multiple UAV flights to analyze the influence of acquisition context, as well as flight and sensor parameters on a managed poplar plantation test plot. The summarized conclusions of this study are presented in Fig. 13. Using an extensive set of comparison data (including field measurements, LiDAR from other sensors and platforms, and satellite-derived products), we assessed the potential of UAV-based LiDAR for forest inventory applications.

For tree height estimation, the performances were generally very good. The results presented here showed excellent correlations with reference datasets and were consistent with expected annual growth rates. A few outliers were observed with the DJI L1 sensor, but above a certain combination of acquisition parameters (flight altitude ≤ 60 m above canopy and point density > 1,000 pts m^{-2}), no significant variation between flights was detected.

For trunk circumference estimation at breast height, results exhibited much greater variability across flights, making robust conclusions more challenging. The most critical factor was the absence of vegetation around tree bases: branch-removal algorithms, adapted from terrestrial LiDAR workflows, performed poorly with DJI L1 point clouds, where using local point density to identify trunks proved largely ineffective. This major contextual parameter explains the poor results observed in all 2025 flights. Nevertheless, it remains possible to use trunk sections other than at breast height (between 0.60 m and 2 m) without compromising result validity. Flight parameters also had a substantial impact, with the best results obtained under conditions similar to those identified for height estimation. The optimal trade-off between data volume and performance was achieved in Flight 8 (1,345 pts m^{-2} at 45 m altitude), which highlighted the benefit of capturing three returns (R^2 = 0.83; RMSE = 13.4 cm; bias = 6.2 cm). Algorithm parameterization also strongly influences outcomes and requires further refinement.**Figure 13.** *Impact of (a) flight parameters and (b) environmental context on the quality of UAV-acquired LiDAR point clouds. This figure is adapted from* Eisenschink et al. (2025) *and extended with findings from the present study.*

The practical utility of UAV-based LiDAR compared to manual field measurements warrants consideration. After initial research and development efforts, UAV-based measurements appear time-efficient: manual circumference measurements for the entire plot required ~ 3 h (potentially reduced with professional tools), whereas UAV data collection took ~ 30 min for preparation and flight, plus ~ 30 min of largely automated data processing. This efficiency gap would likely widen on larger plots, favoring UAV-based LiDAR. However, hardware costs (drone and high-performance computer), operator expertise, and flight authorizations represent significant constraints.

Overall, UAV-based LiDAR appears particularly valuable for tree height estimation, a parameter that is both difficult to measure manually and reliably derived here.

While this study focused on a single species over a small, well-maintained area under optimal conditions, future work should extend these methods to other homogeneous plantation species, such as pines with similar morphologies. In contrast, mixed-species forests with understory vegetation and

complex, irregular tree forms (e.g., oaks) are expected to present greater challenges and reduced performance.

Finally, the two metrics extracted here (tree height and trunk circumference) are key variables for biomass estimation, often serving as inputs to empirical allometric equations. Future work should explore these relationships and compare UAV-derived estimates with timber volume data held by forest managers, fostering dialogue with silvicultural practitioners.

Declarations

Declaration of generative AI and AI-assisted technologies in the manuscript preparation process:

During the preparation of this manuscript, the authors used ChatGPT (OpenAI) and DeepL to support translation and language editing in English. All scientific content, analyses, interpretations, and conclusions were produced by the authors. The authors reviewed and edited the text as needed and take full responsibility for the content of the published article.

Funding:

This work was supported by the ALAMOD (ANR-22-PEXF-002-projet ALAMOD) projects of the French National Research Agency, under the France2030 program, in the framework of the national PEPR “FAIRCARBON” program and by the European Union through the Interreg SUDOE SocialForest project.

Author Contribution

C.B. developed required computer programs, analyzed the data, and composed the manuscript. F.B. provided the UAV data and designed the experiments. F.F. and F.B. supervised the research project, advised with the research, and contributed in composing the manuscript. M.S. provided the FORMS-T data and analysis, and helped improve the writing.

Acknowledgement

We would like to thank Pierre Valerio and Parera (especially Mr. Stéphane Gasset) for providing the terrestrial LiDAR (TLS) data, Laurent Barbat for granting access to the study area, and the Professional Licence GGAT (IUT Auch – University of Toulouse) for lending equipment as part of educational training projects.

Data Availability

The UAV LiDAR datasets will be available in a Data paper. Ground-based LiDAR and FORMS-T datasets are available from the authors upon request.

References

1. Balado J, Arias P, Lorenzo H, Meijide-Rodríguez A (2021) Disturbance Analysis in the Classification of Objects Obtained from Urban LiDAR Point Clouds with Convolutional Neural Networks. Remote Sens 13:2135. https://doi.org/10.3390/rs13112135
2. Binot J-M, Pothier D, Lebel J (1995) Comparison of relative accuracy and time requirement between the caliper, the diameter tape and an electronic tree measuring fork. Forestry Chron 71:197–200. https://doi.org/10.5558/tfc71197-2
3. Bragg DC (2014) Accurately Measuring the Height of (Real) Forest Trees. J Forest 112:51–54. https://doi.org/10.5849/jof.13-065
4. Brede B, Lau A, Bartholomeus H, Kooistra L (2017) Comparing RIEGL RiCOPTER UAV LiDAR Derived Canopy Height and DBH with Terrestrial LiDAR. Sensors 17:2371. https://doi.org/10.3390/s17102371
5. Calders K, Verbeeck H, Burt A, Origo N, Nightingale J, Malhi Y, Wilkes P, Raumonen P, Bunce RGH, Disney M (2022) Laser scanning reveals potential underestimation of biomass carbon in temperate forest. Ecol Sol Evid 3:e12197. https://doi.org/10.1002/2688-8319.12197
6. Clark NA, Wynne RH, Schmoldt DL, Winn M (2000) An assessment of the utility of a non-metric digital camera for measuring standing trees. Comput Electron Agric 28:151–169. https://doi.org/10.1016/S0168-1699(00)00125-3
7. Daeyeol K, Song Y, Kim H, Kwon O, Yeon Y-K, Lim T (2025) Airborne multi-seasonal LiDAR and hyperspectral data integration for individual tree-level classification in urban green spaces at city scale. Int J Appl Earth Obs Geoinf 136:104319. https://doi.org/10.1016/j.jag.2024.104319
8. Dalla Corte AP, Rex FE, Almeida DRAD, Sanquetta CR, Silva CA, Moura MM, Wilkinson B, Zambrano AMA, Cunha Neto EMD, Veras HFP, Moraes AD, Klauberg C, Mohan M, Cardil A, Broadbent EN 2020. Measuring Individual Tree Diameter and Height Using GatorEye High-Density UAV-Lidar in an Integrated Crop-Livestock-Forest System. Remote Sens 12, 863. https://doi.org/10.3390/rs12050863
9. Dickmann D, Stuart K (1983) Culture of hybrid poplars in northeastern North America, East Lansing. Michigan State University, ed, Department of Forestry
10. Dong P, Chen Q (2017) LiDAR Remote Sensing and Applications, 1st ed. CRC Press, Boca Raton, FL: Taylor & Francis, 2018. https://doi.org/10.4324/9781351233354
11. Duncanson LI, Cook BD, Hurtt GC, Dubayah RO (2014) An efficient, multi-layered crown delineation algorithm for mapping individual tree structure across multiple ecosystems. Remote Sens Environ 154:378–386. https://doi.org/10.1016/j.rse.2013.07.044

12. Eisenschink PM, Obermeier WA, Zerres VHD, Suerbaum AM, Lehnert LW (2025) Forest variables from LiDAR: Drone flight parameters impact the detection of tree stems and diameter estimates. Ecol Inf 88:103127. https://doi.org/10.1016/j.ecoinf.2025.103127
13. Evans DL, Roberts SD, Parker RC (2006) LiDAR A new tool for forest measurements? Forestry Chron 82:211–218. https://doi.org/10.5558/tfc82211-2
14. Eysn L, Hollaus M, Lindberg E, Berger F, Monnet J-M, Dalponte M, Kobal M, Pellegrini M, Lingua E, Mongus D, Pfeifer N (2015) A Benchmark of Lidar-Based Single Tree Detection Methods Using Heterogeneous Forest Data from the Alpine Space. Forests 6:1721–1747. https://doi.org/10.3390/f6051721
15. Feng B, Nie S, Wang C, Xi X, Wang J, Zhou G, Wang H (2022) Exploring the Potential of UAV LiDAR Data for Trunk Point Extraction and Direct DBH Measurement. Remote Sens 14:2753. https://doi.org/10.3390/rs14122753
16. Ferraz A, Saatchi S, Mallet C, Meyer V (2016) Lidar detection of individual tree size in tropical forests. Remote Sens Environ 183:318–333. https://doi.org/10.1016/j.rse.2016.05.028
17. Gehring C, Park S, Denich M (2008) Close relationship between diameters at 30cm height and at breast height (DBH). Acta Amaz 38:71–76. https://doi.org/10.1590/S0044-59672008000100008
18. Grosenbaugh LR (1963) Optical Dendrometers For Out-Of-Reach Diameters: A Conspectus And Some New Theory. For Sci 9:a0001–47. https://doi.org/10.1093/forestscience/9.s1.a0001
19. Guenther M, Heenkenda MK, Leblon B, Morris D, Freeburn J (2024a) Estimating Tree Diameter at Breast Height (DBH) Using iPad Pro LiDAR Sensor in Boreal Forests. Can J Remote Sens 50:2295470. https://doi.org/10.1080/07038992.2023.2295470
20. Guenther M, Heenkenda MK, Morris D, Leblon B (2024b) Tree Diameter at Breast Height (DBH) Estimation Using an iPad Pro LiDAR Scanner: A Case Study in Boreal Forests. Ont Can Forests 15:214. https://doi.org/10.3390/f15010214
21. Gülci S, Yurtseven H, Akay AO, Akgul M (2023) Measuring tree diameter using a LiDAR-equipped smartphone: a comparison of smartphone- and caliper-based DBH. Environ Monit Assess 195:678. https://doi.org/10.1007/s10661-023-11366-8
22. Hamraz H, Contreras MA, Zhang J (2017) Forest understory trees can be segmented accurately within sufficiently dense airborne laser scanning point clouds. Sci Rep 7:6770. https://doi.org/10.1038/s41598-017-07200-0
23. Heo HK, Lee DK, Park JH, Thorne JH (2019) Estimating the heights and diameters at breast height of trees in an urban park and along a street using mobile LiDAR. Landsc Ecol Eng 15:253–263. https://doi.org/10.1007/s11355-019-00379-6
24. Hopkinson C, Chasmer L, Young-Pow C, Treitz P (2004) Assessing forest metrics with a ground-based scanning lidar. Can J Res 34:573–583. https://doi.org/10.1139/x03-225
25. Houghton RA (2005) Aboveground Forest Biomass and the Global Carbon Balance. Glob Change Biol 11:945–958. https://doi.org/10.1111/j.1365-2486.2005.00955.x

26. Huang H, Li Z, Gong P, Cheng X, Clinton N, Cao C, Ni W, Wang L (2011) Automated Methods for Measuring DBH and Tree Heights with a Commercial Scanning Lidar. photogramm eng remote sensing. 77:219–227. https://doi.org/10.14358/PERS.77.3.219
27. Hui Z, Lin L, Jin S, Xia Y, Ziggah YY (2024) A Reliable DBH Estimation Method Using Terrestrial LiDAR Points through Polar Coordinate Transformation and Progressive Outlier Removal. Forests 15:1031. https://doi.org/10.3390/f15061031
28. Hyyppä J, Hyyppä H, Leckie D, Gougeon F, Yu X, Maltamo M (2008) Review of methods of small-footprint airborne laser scanning for extracting forest inventory data in boreal forests. Int J Remote Sens 29:1339–1366. https://doi.org/10.1080/01431160701736489
29. Jenkins JC, Chojnacky DC, Heath LS, Birdsey RA (2003) National-Scale Biomass Estimators for United States Tree Species. For Sci 49:12–35. https://doi.org/10.1093/forestscience/49.1.12
30. Keeland BD, Sharitz RR (1993) Accuracy of tree growth measurements using dendrometer bands. Can J Res 23:2454–2457. https://doi.org/10.1139/x93-304
31. Kumar L, Mutanga O (2017) Remote Sensing of Above-Ground Biomass. Remote Sens 9:935. https://doi.org/10.3390/rs9090935
32. Leite R, Silva C, Mohan M, Cardil A, Almeida D, Carvalho S, Jaafar W, Guerra-Hernández J, Weiskittel A, Hudak A, Broadbent E, Prata G, Valbuena R, Leite H, Taquetti M, Soares A, Scolforo H, Amaral C, Corte D, Klauberg A, C (2020) Individual Tree Attribute Estimation and Uniformity Assessment in Fast-Growing Eucalyptus spp. Forest Plantations Using Lidar and Linear Mixed-Effects Models. Remote Sens 12:3599. https://doi.org/10.3390/rs12213599
33. Li L, Wei L, Li N, Zhang S, Wu Z, Dong M, Chen Y (2024) Extracting the DBH of Moso Bamboo Forests Using LiDAR: Parameter Optimization and Accuracy Evaluation. Forests 15:804. https://doi.org/10.3390/f15050804
34. Liang X, Kankare V, Hyyppä J, Wang Y, Kukko A, Haggrén H, Yu X, Kaartinen H, Jaakkola A, Guan F, Holopainen M, Vastaranta M (2016) Terrestrial laser scanning in forest inventories. ISPRS J Photogrammetry Remote Sens 115:63–77. https://doi.org/10.1016/j.isprsjprs.2016.01.006
35. Liao K, Li Y, Zou B, Li D, Lu D (2022) Examining the Role of UAV Lidar Data in Improving Tree Volume Calculation Accuracy. Remote Sens 14:4410. https://doi.org/10.3390/rs14174410
36. Liu G, Wang J, Dong P, Chen Y, Liu Z (2018) Estimating Individual Tree Height and Diameter at Breast Height (DBH) from Terrestrial Laser Scanning (TLS) Data at Plot Level. Forests 9:398. https://doi.org/10.3390/f9070398
37. Liu L, Zhang A, Xiao S, Hu S, He N, Pang H, Zhang X, Yang S (2021) Single Tree Segmentation and Diameter at Breast Height Estimation With Mobile LiDAR. IEEE Access 9:24314–24325. https://doi.org/10.1109/ACCESS.2021.3056877
38. Lu D, Chen Q, Wang G, Liu L, Li G, Moran E (2016) A survey of remote sensing-based aboveground biomass estimation methods in forest ecosystems. Int J Digit Earth 9:63–105. https://doi.org/10.1080/17538947.2014.990526

39. Maclean GA, Krabill WB (1986) Gross-Merchantable Timber Volume Estimation Using an Airborne Lidar System. Can J Remote Sens 12:7–18. https://doi.org/10.1080/07038992.1986.10855092
40. Mapuru M, Xulu S, Gebreslasie M (2023) Remote Sensing Applications in Monitoring Poplars: A Review. Forests 14:2301. https://doi.org/10.3390/f14122301
41. Moe KT, Owari T, Furuya N, Hiroshima T, Morimoto J (2020) Application of UAV Photogrammetry with LiDAR Data to Facilitate the Estimation of Tree Locations and DBH Values for High-Value Timber Species in Northern Japanese Mixed-Wood Forests. Remote Sens 12:2865. https://doi.org/10.3390/rs12172865
42. Moorthy I, Miller JR, Berni JAJ, Zarco-Tejada P, Hu B, Chen J (2011) Field characterization of olive (Olea europaea L.) tree crown architecture using terrestrial laser scanning data. Agric For Meteorol 151:204–214. https://doi.org/10.1016/j.agrformet.2010.10.005
43. Muukkonen P (2007) Generalized allometric volume and biomass equations for some tree species in Europe. Eur J For Res 126:157–166. https://doi.org/10.1007/s10342-007-0168-4
44. Neuville R, Bates JS, Jonard F (2021) Estimating Forest Structure from UAV-Mounted LiDAR Point Cloud Using Machine Learning. Remote Sens 13:352. https://doi.org/10.3390/rs13030352
45. Persson A, Holmgren J, Söderman U (2002) Detecting and measuring individual trees using an airborne laser scanner. Photogram Eng Remote Sens 68:925–932
46. Popescu SC (2007) Estimating biomass of individual pine trees using airborne lidar. Biomass Bioenergy 31:646–655. https://doi.org/10.1016/j.biombioe.2007.06.022
47. Pretzsch H (2009) Forest Dynamics, Growth and Yield: From Measurement to Model. Springer, Berlin Heidelberg, Berlin, Heidelberg. https://doi.org/10.1007/978-3-540-88307-4
48. Proudman A, Ramezani M, Fallon M (2021) Online Estimation of Diameter at Breast Height (DBH) of Forest Trees Using a Handheld LiDAR, in: 2021 European Conference on Mobile Robots (ECMR). Presented at the 2021 European Conference on Mobile Robots (ECMR), IEEE, Bonn, Germany, pp. 1–7. https://doi.org/10.1109/ECMR50962.2021.9568814
49. Puente I, González-Jorge H, Martínez-Sánchez J, Arias P (2013) Review of mobile mapping and surveying technologies. Measurement 46:2127–2145. https://doi.org/10.1016/j.measurement.2013.03.006
50. Saarinen N, Kankare V, Vastaranta M, Luoma V, Pyörälä J, Tanhuanpää T, Liang X, Kaartinen H, Kukko A, Jaakkola A, Yu X, Holopainen M, Hyyppä J (2017) Feasibility of Terrestrial laser scanning for collecting stem volume information from single trees. ISPRS J Photogrammetry Remote Sens 123:140–158. https://doi.org/10.1016/j.isprsjprs.2016.11.012
51. Schwartz M, Ciais P, De Truchis A, Chave J, Ottlé C, Vega C, Wigneron J-P, Nicolas M, Jouaber S, Liu S, Brandt M, Fayad I (2023) Forest Multiple Source height, wood volume, and biomass maps in France at 10 to 30 m resolution based on Sentinel-1, Sentinel-2, and Global Ecosystem Dynamics Investigation (GEDI) data with a deep learning approach. Earth Syst Sci Data 15:4927–4945. https://doi.org/10.5194/essd-15-4927-2023

52. Schwartz M, Ciais P, Sean E, De Truchis A, Vega C, Besic N, Fayad I, Wigneron J-P, Brood S, Pelissier-Tanon A, Pauls J, Belouze G, Xu Y (2025) Retrieving yearly forest growth from satellite data: A deep learning based approach. Remote Sens Environ 330:114959. https://doi.org/10.1016/j.rse.2025.114959
53. Temesgen H, Affleck D, Poudel K, Gray A, Sessions J (2015) A review of the challenges and opportunities in estimating above ground forest biomass using tree-level models. Scand J For Res 1–10. https://doi.org/10.1080/02827581.2015.1012114
54. Tolan J, Yang H-I, Nosarzewski B, Couairon G, Vo HV, Brandt J, Spore J, Majumdar S, Haziza D, Vamaraju J, Moutakanni T, Bojanowski P, Johns T, White B, Tiecke T, Couprie C (2024) Very high resolution canopy height maps from RGB imagery using self-supervised vision transformer and convolutional decoder trained on aerial lidar. Remote Sens Environ 300:113888. https://doi.org/10.1016/j.rse.2023.113888
55. Geological Survey US (2024) Lidar Mapping Report for the U.S. Geological Survey
56. Vashum KT, Jayakumar S (2012) Methods to estimate above-ground biomass and carbon stock in natural forests-a review. J Ecosyst Ecography 2:1–7
57. Wang F, Heenkenda MK, Freeburn JT (2022) Estimating tree Diameter at Breast Height (DBH) using an iPad Pro LiDAR sensor. Remote Sens Lett 13:568–578. https://doi.org/10.1080/2150704X.2022.2051635
58. West PW (2015) Tree and Forest Measurement. Springer International Publishing, Cham. https://doi.org/10.1007/978-3-319-14708-6
59. Wu J, Yao W, Choi S, Park T, Myneni RB (2015) A Comparative Study of Predicting DBH and Stem Volume of Individual Trees in a Temperate Forest Using Airborne Waveform LiDAR. IEEE Geosci Remote Sens Lett 12:2267–2271. https://doi.org/10.1109/LGRS.2015.2466464
60. Xie Y, Yang T, Wang X, Chen X, Pang S, Hu J, Wang A, Chen L, Shen Z (2022) Applying a Portable Backpack Lidar to Measure and Locate Trees in a Nature Forest Plot: Accuracy and Error Analyses. Remote Sens 14:1806. https://doi.org/10.3390/rs14081806
61. Yang Z, Liu Q, Luo P, Ye Q, Duan G, Sharma RP, Zhang H, Wang G, Fu L (2020) Prediction of Individual Tree Diameter and Height to Crown Base Using Nonlinear Simultaneous Regression and Airborne LiDAR Data. Remote Sens 12:2238. https://doi.org/10.3390/rs12142238
62. Yun T, Jiang K, Li G, Eichhorn MP, Fan J, Liu F, Chen B, An F, Cao L (2021) Individual tree crown segmentation from airborne LiDAR data using a novel Gaussian filter and energy function minimization-based approach. Remote Sens Environ 256:112307. https://doi.org/10.1016/j.rse.2021.112307
63. Zolanvari SMI, Ruano S, Rana A, Cummins A, da Silva RE, Rahbar M, Smolic A (2019) DublinCity: Annotated LiDAR Point Cloud and its Applications. https://doi.org/10.48550/ARXIV.1909.03613
64. Zolkos SG, Goetz SJ, Dubayah R (2013) A meta-analysis of terrestrial aboveground biomass estimation using lidar remote sensing. Remote Sens Environ 128:289–298. https://doi.org/10.1016/j.rse.2012.10.017

Figures

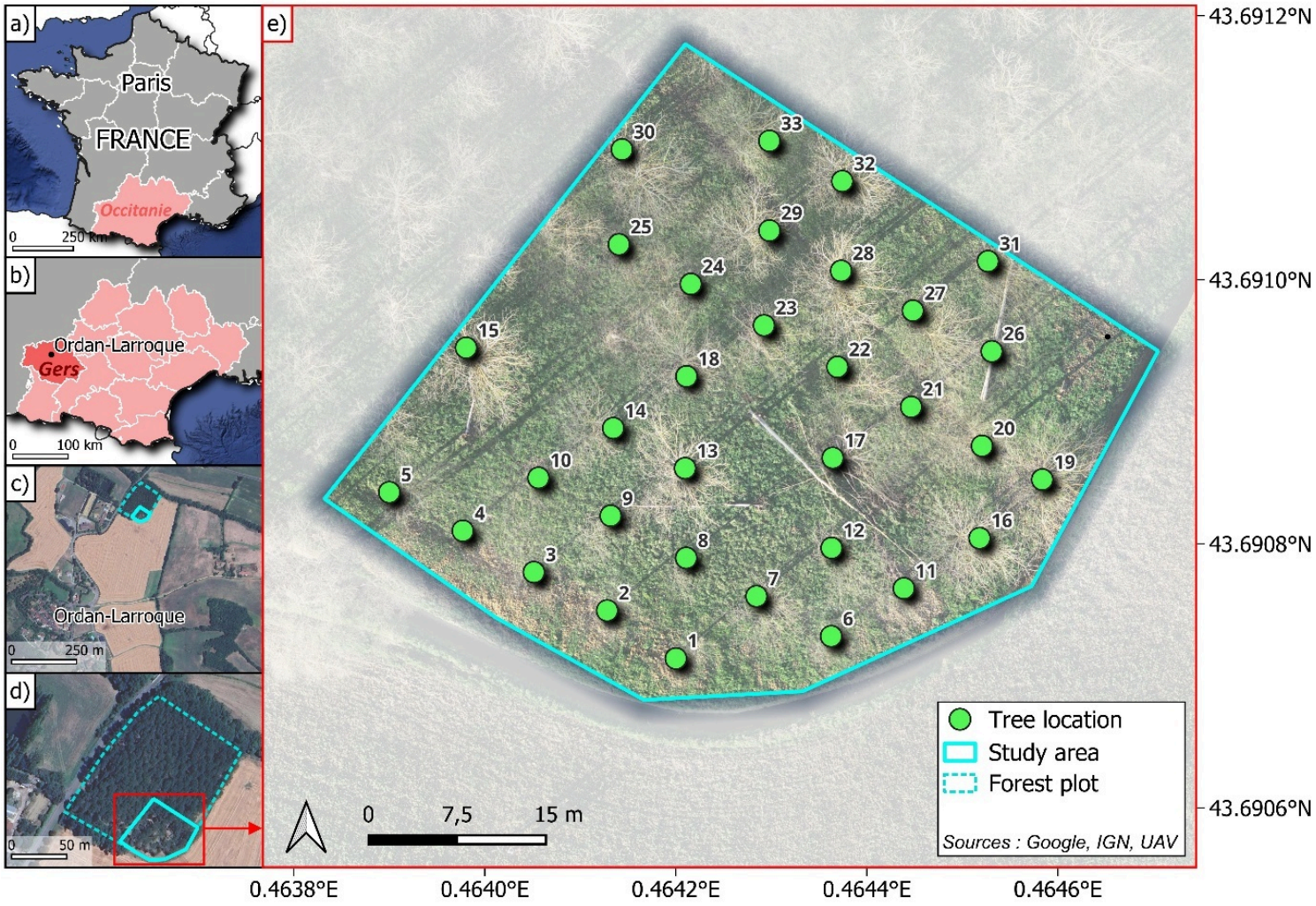


Figure 1

Overview of the study area: (a) location within France of Occitanie region; (b) location within the Occitanie region. The forest plot is shown on Google Satellite images in (c) and (d). A detailed view of the study area, including tree locations, is provided in (e), with an UAV orthoimage as background.

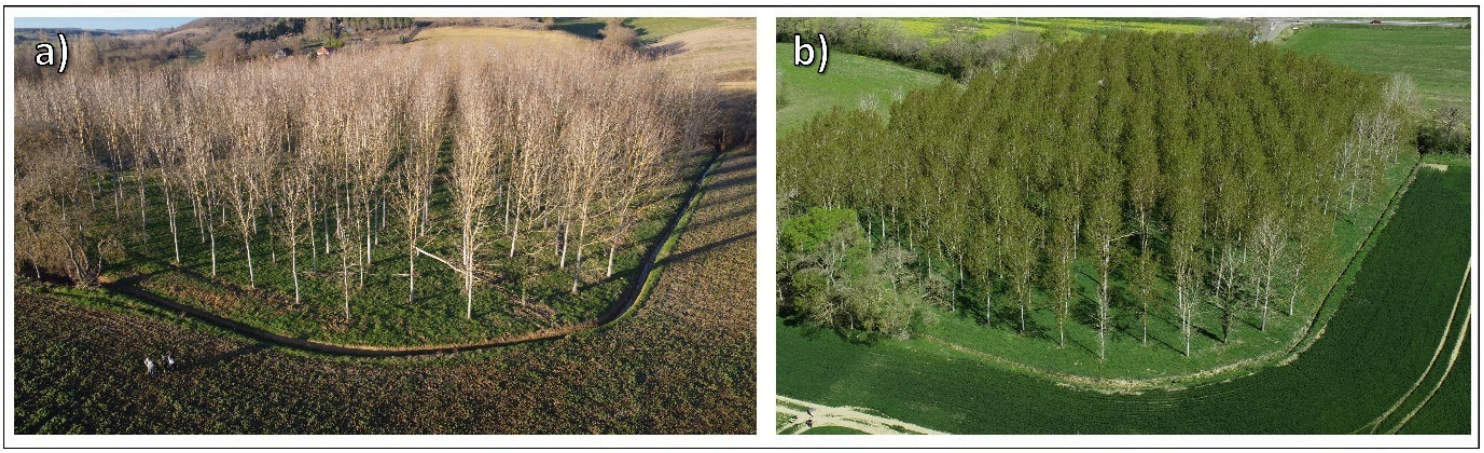


Figure 2

Photographs of the study site on 23 January 2024 (a) and 09 April 2025 (b), showing leaf emergence.

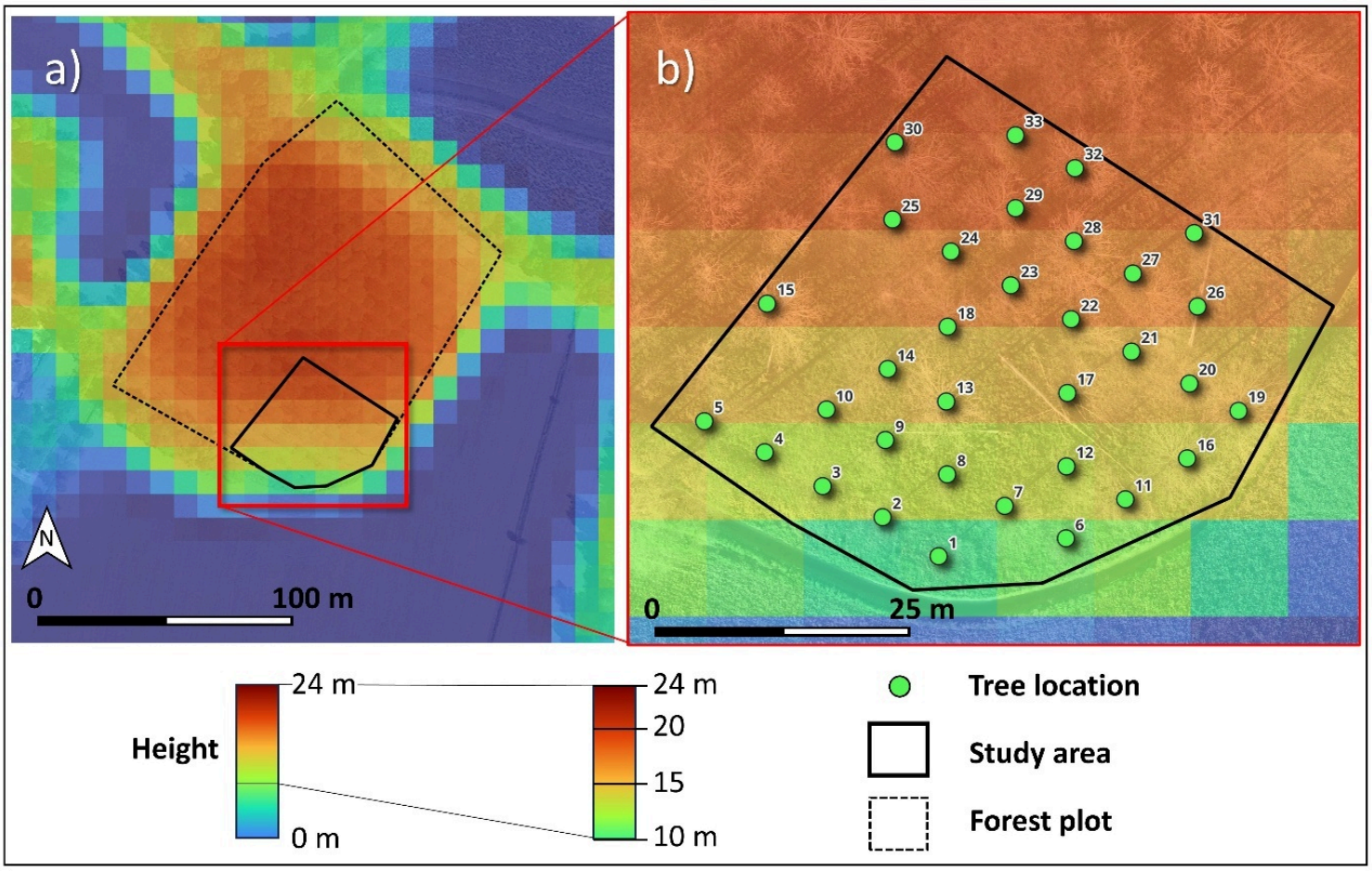


Figure 3

Overview of the FORMS-T dataset (2024) across the entire forest plot (a) and the study area (b).

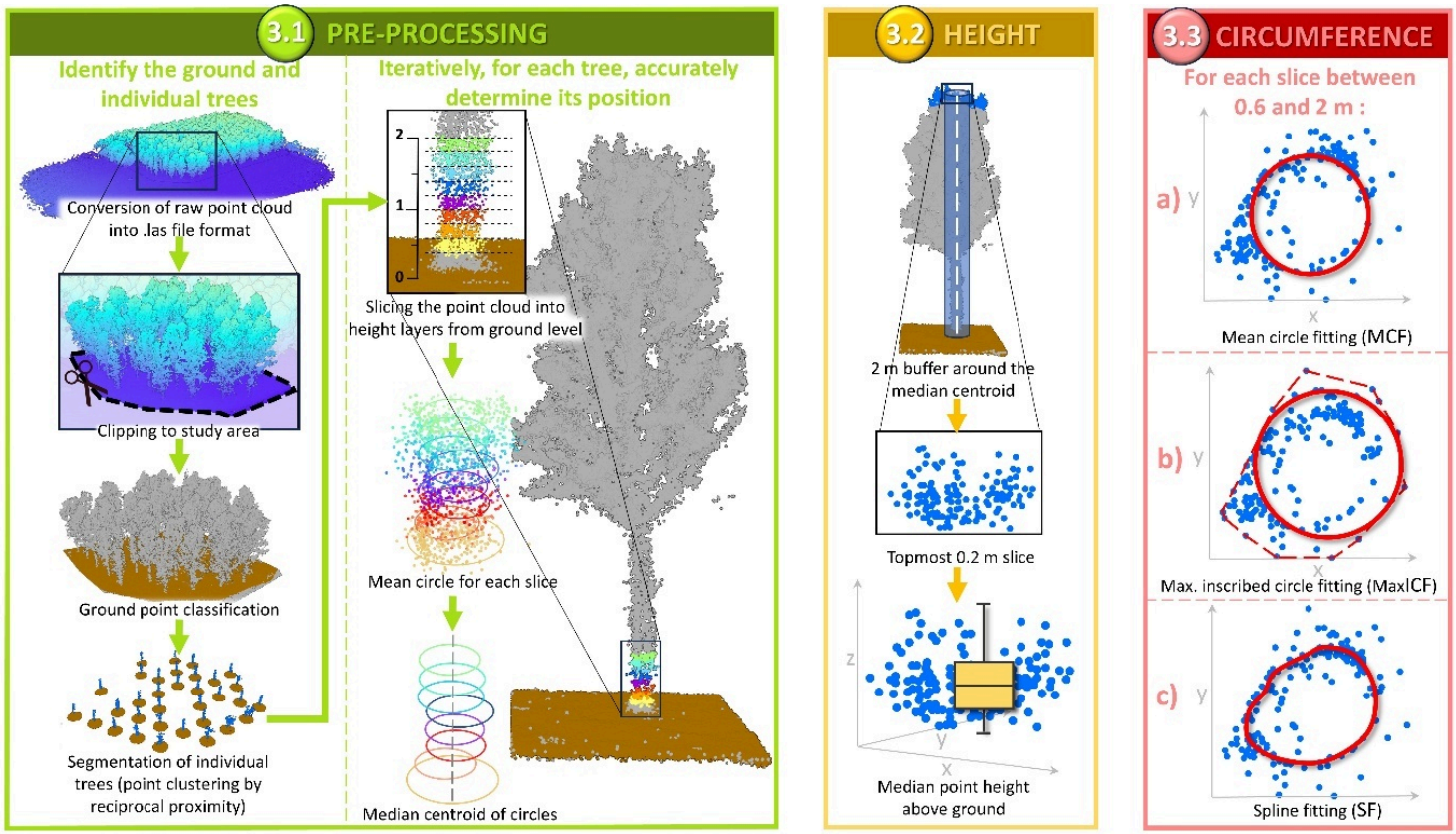


Figure 4

Workflow for processing LiDAR data to extract height and circumference of individual trees; Pre-processing (3.1), Computation of canopy heights (3.2) and trunk circumferences with 3 different methods: Mean Circle Fitting (MCF), Maximum Inscribed Circle Fitting (MaxICF), and Spline Fitting (SF) (3.3).

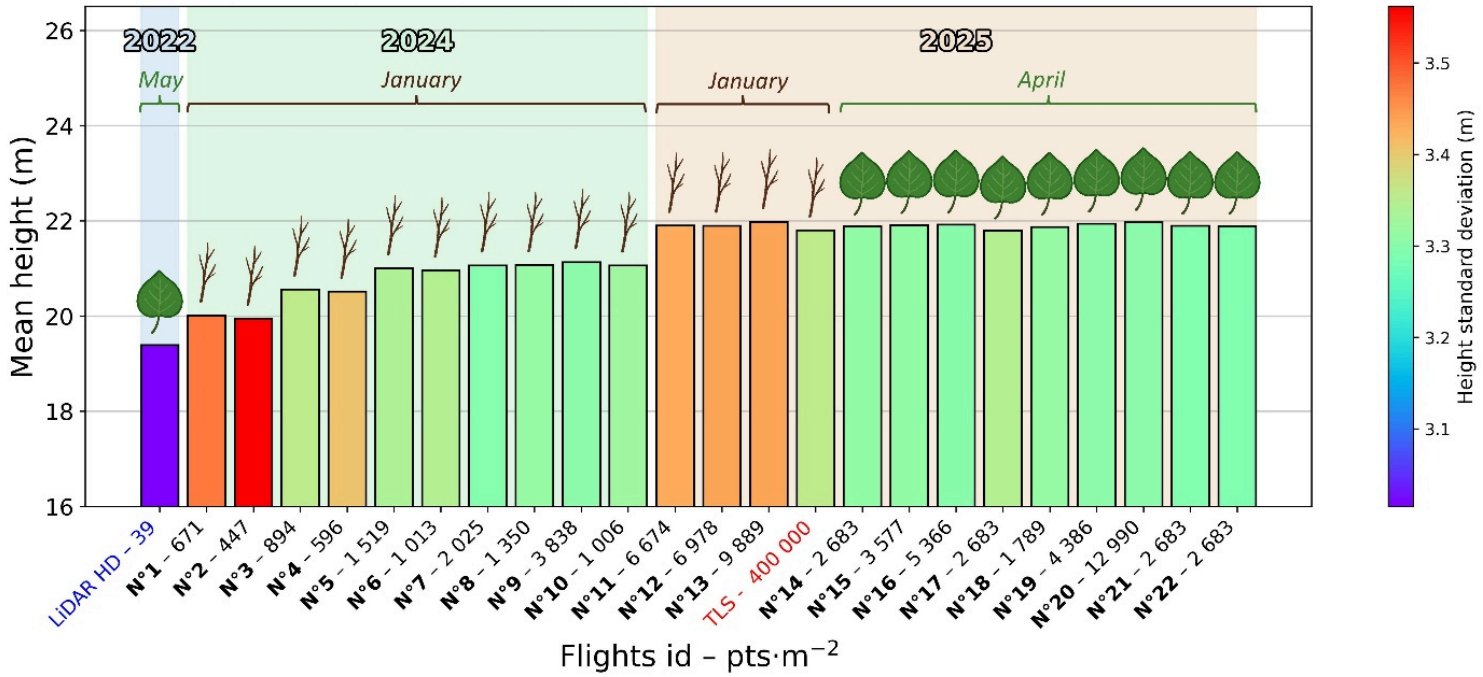


Figure 5

Mean canopy heights derived from all LiDAR datasets, with associated standard deviations. The average point density (points.m⁻²) for each flight is indicated below. The presence (May 2022 and April 2025, symbolized by a green leaf) or absence (January 2024 and 2025, symbolized by a brown branch) of foliage on branches at the time of data acquisition is also noted.

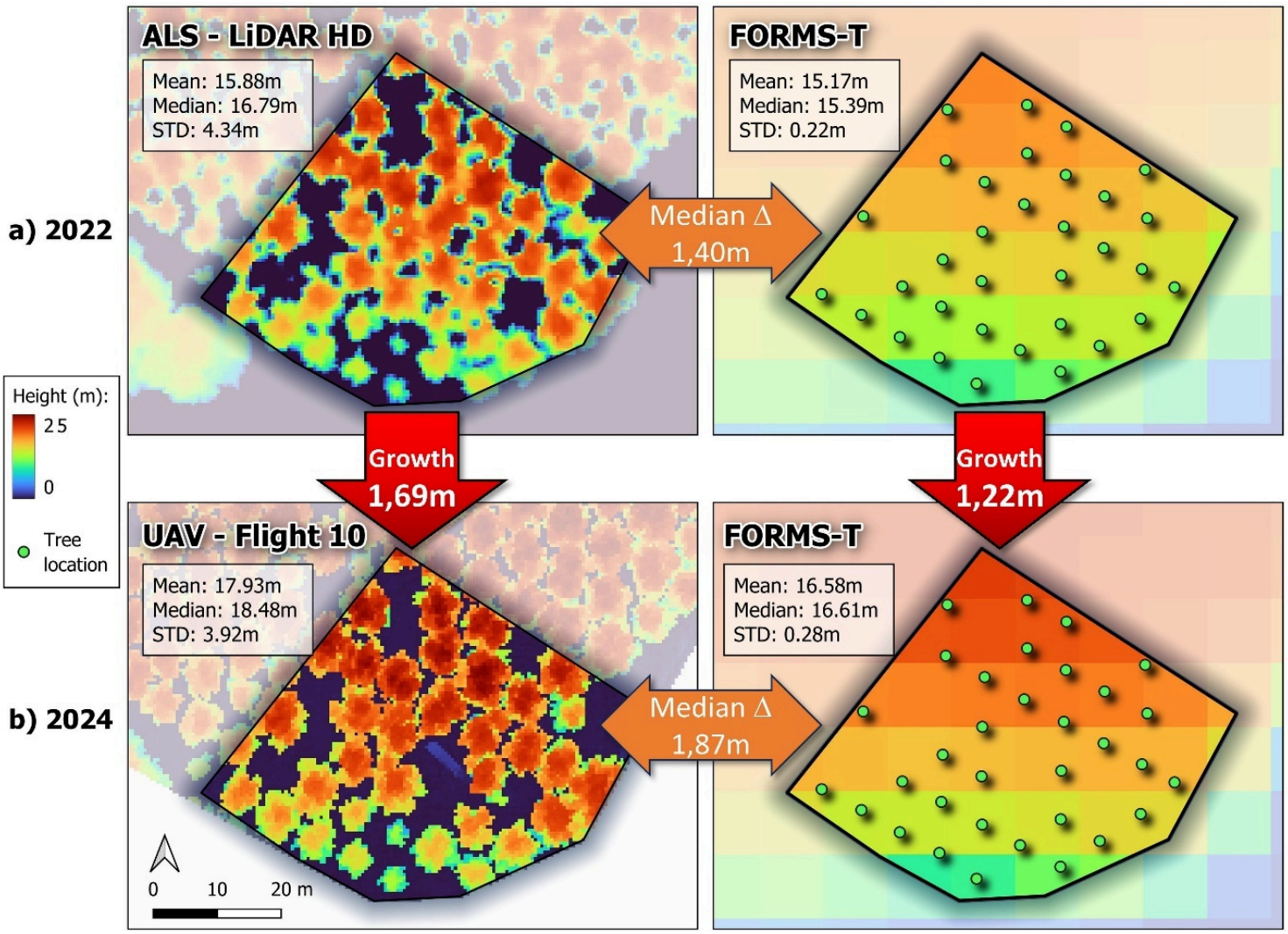


Figure 6

Comparison maps between (a) the 2022 DHM derived from HD LiDAR and the FORMS-T product from the same year, and (b) the 2024 DHM generated from UAV LiDAR data (Flight 10) and FORMS-T product from the same year. Summary statistics for each raster are reported over the study area, along with the mean height growth observed in the plot between 2022 and 2024 based on these datasets.

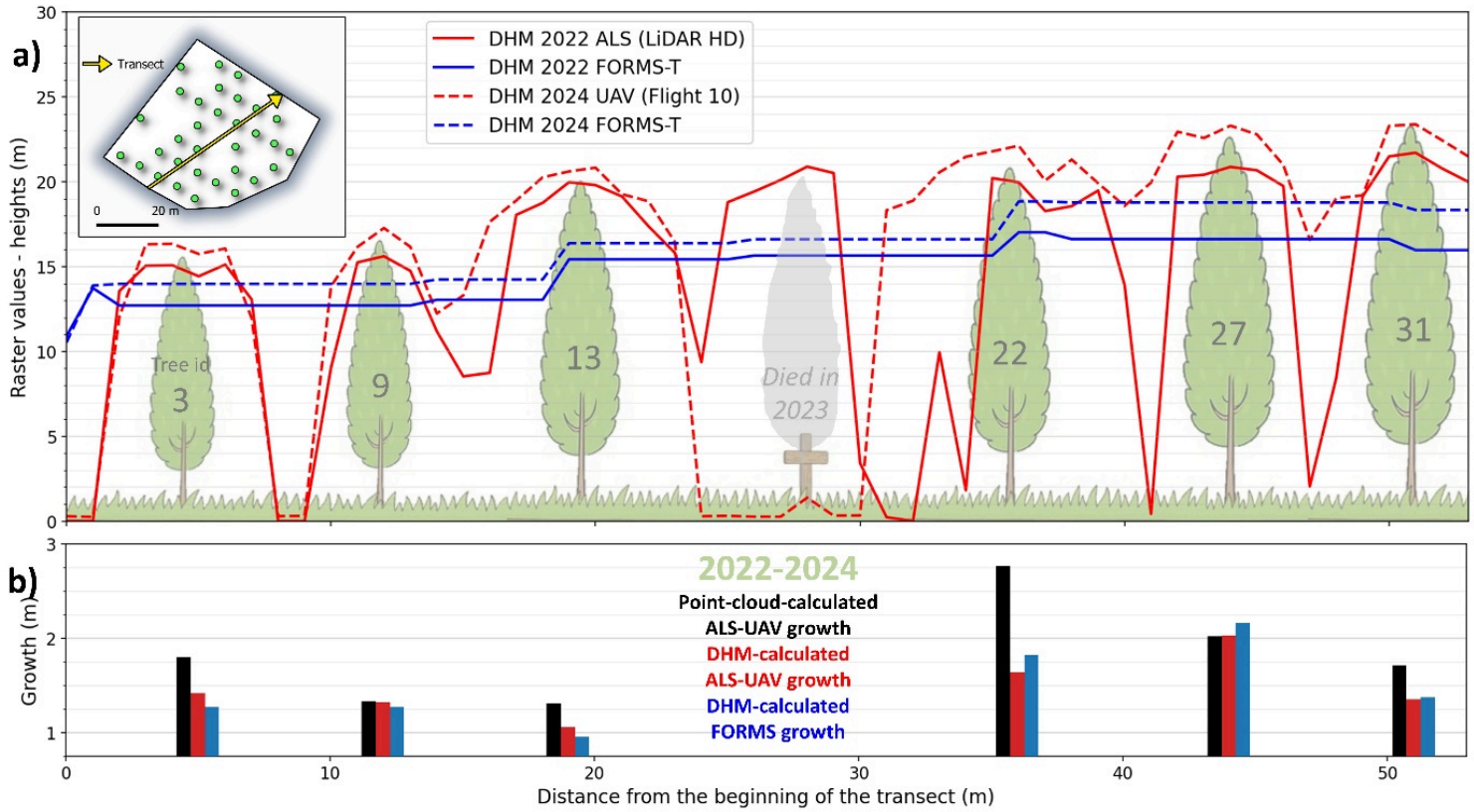


Figure 7

(a) Comparison of height values from the different DHMs sampled along a transect, represented in the map subplot; the trees located beneath the transect are shown in the background at their heights estimated in 2022 by the HD LiDAR data. (b) Growth values computed from these datasets for the six trees located along the transect.

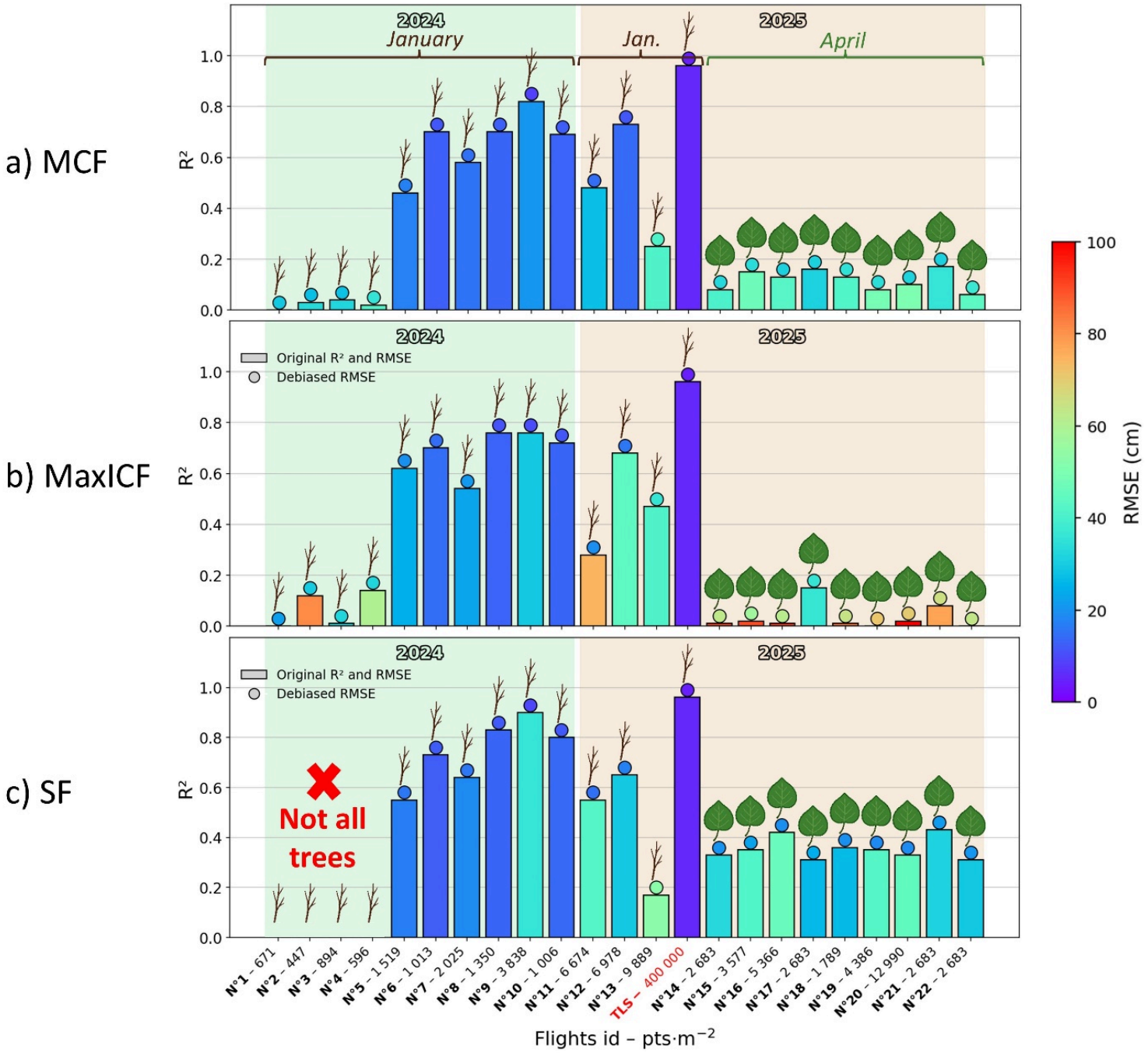


Figure 8

Comparative performance of all LiDAR datasets for (a) $C_{MCF,}$ (b)$C_{MaxICF,}$ and (c) C_{SF},when compared to field measurement. The R² values are shown on the y-axis, and bars are color-coded according to RMSE. Debiased RMSE is also shown on colored dots, above the bars. The presence (May 2022 and April 2025, symbolized by a green leaf) or absence (January 2024 and 2025, symbolized by a brown branch) of foliage on branches at the time of data acquisition is also noted.

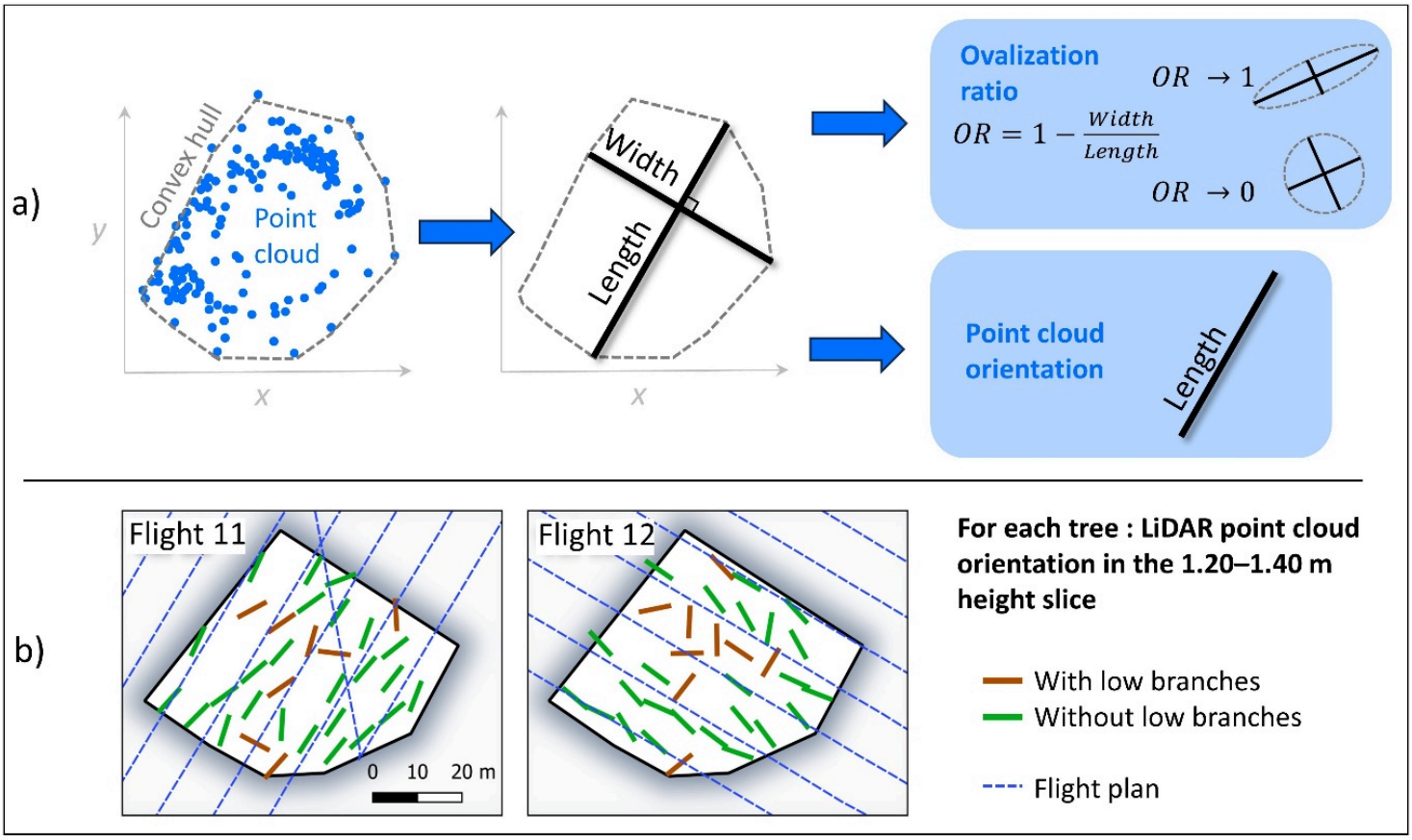


Figure 9

(a) Metrics used to quantify trunk point cloud ovalization and orientation within a defined height slice, and (b) Orientation of point clouds within the 1.20–1.40 m slice for flights 11 and 12 with similar characteristics, except for their flight plan angles. The map illustrates the orientation of point cloud elongation for each tree (i.e., the longest segment within the convex hull of the point cloud). Trees with low branches, which may distort cloud shape and interfere with analysis, are indicated separately.

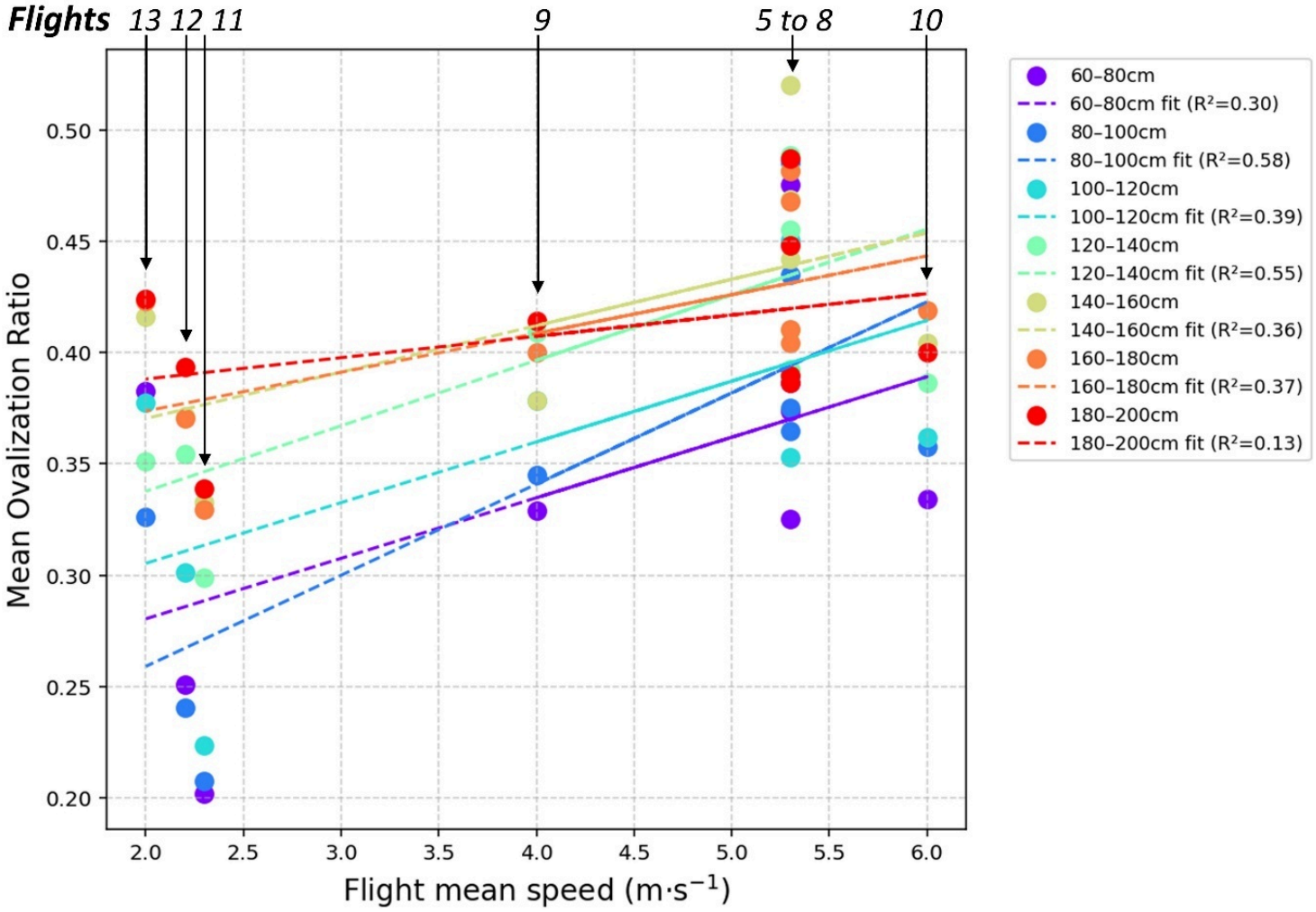


Figure 10

Ovalization ratio vs. mean flight speed across different heights (flights executed during winter 2024 and winter 2025).

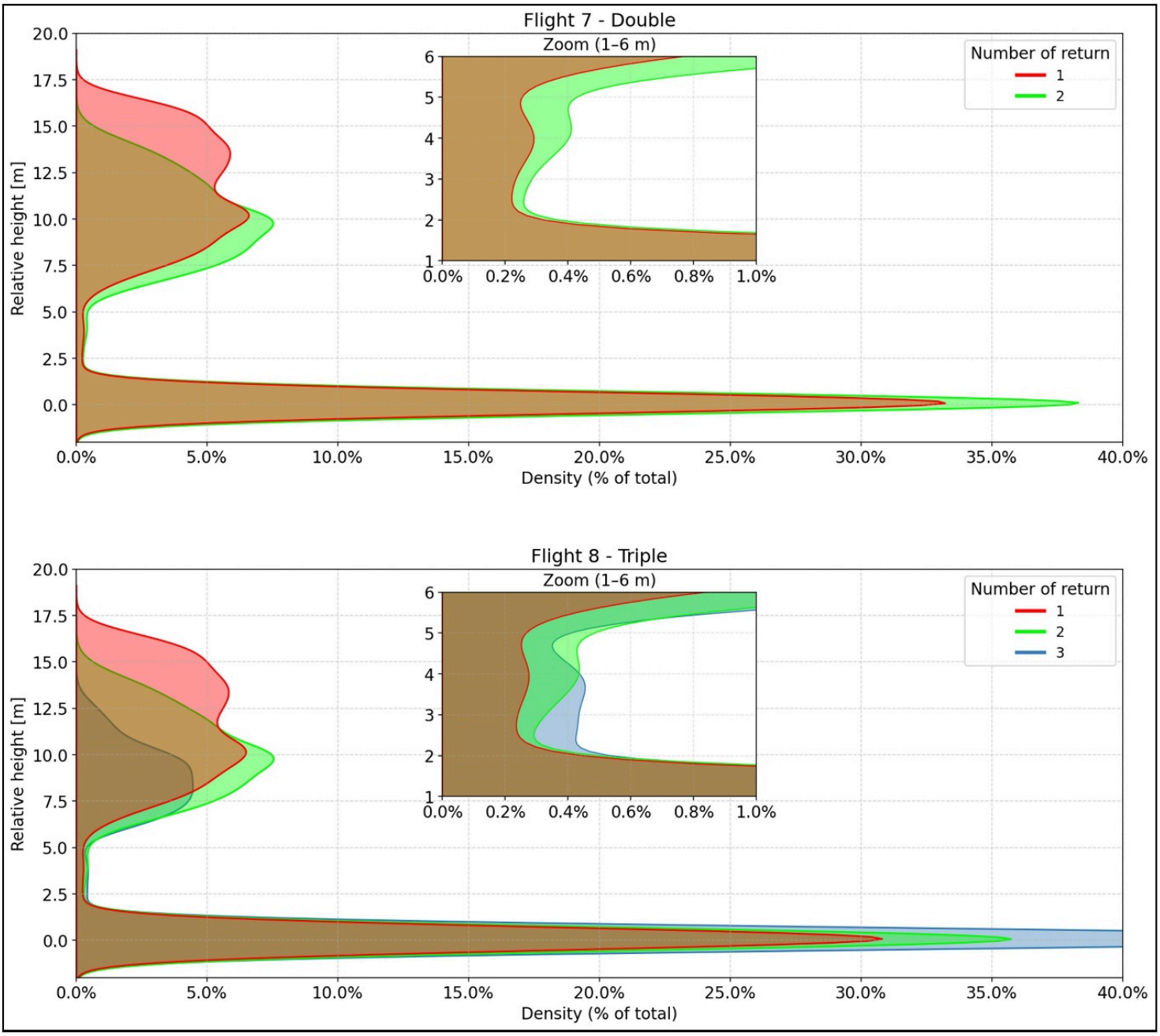


Figure 11

Comparative distribution of LiDAR return density as a function of relative height for a test tree in Flight 7 (dual return mode) and Flight 8 (triple). The inset highlights the 1–6 m slice corresponding to the tree trunk.

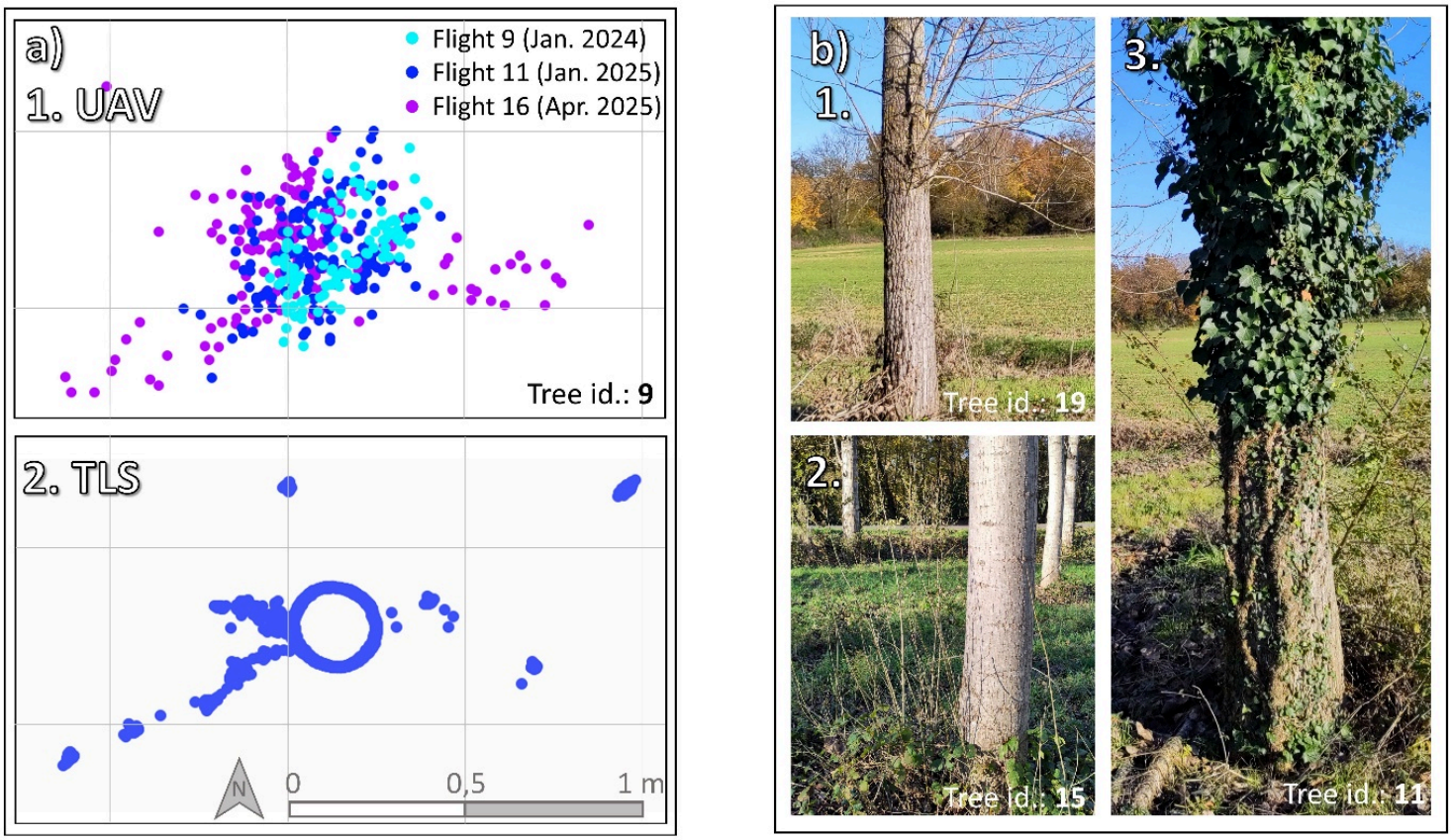


Figure 12

(a) Evolution of DJI L1 LiDAR point clouds within the 1.20–1.40 m slice for Tree 9 across three consecutive UAV acquisitions (a.1), showing the effect of basal vegetation growth, compared to the MS-96 terrestrial LiDAR point cloud (a.2). Images of trees 19, 15 and 11 (b), taken in January 2025, illustrate examples of vegetation interfering with UAV-based LiDAR trunk definition: low branches (b.1), basal regrowth (b.2), and ivy (b.3).

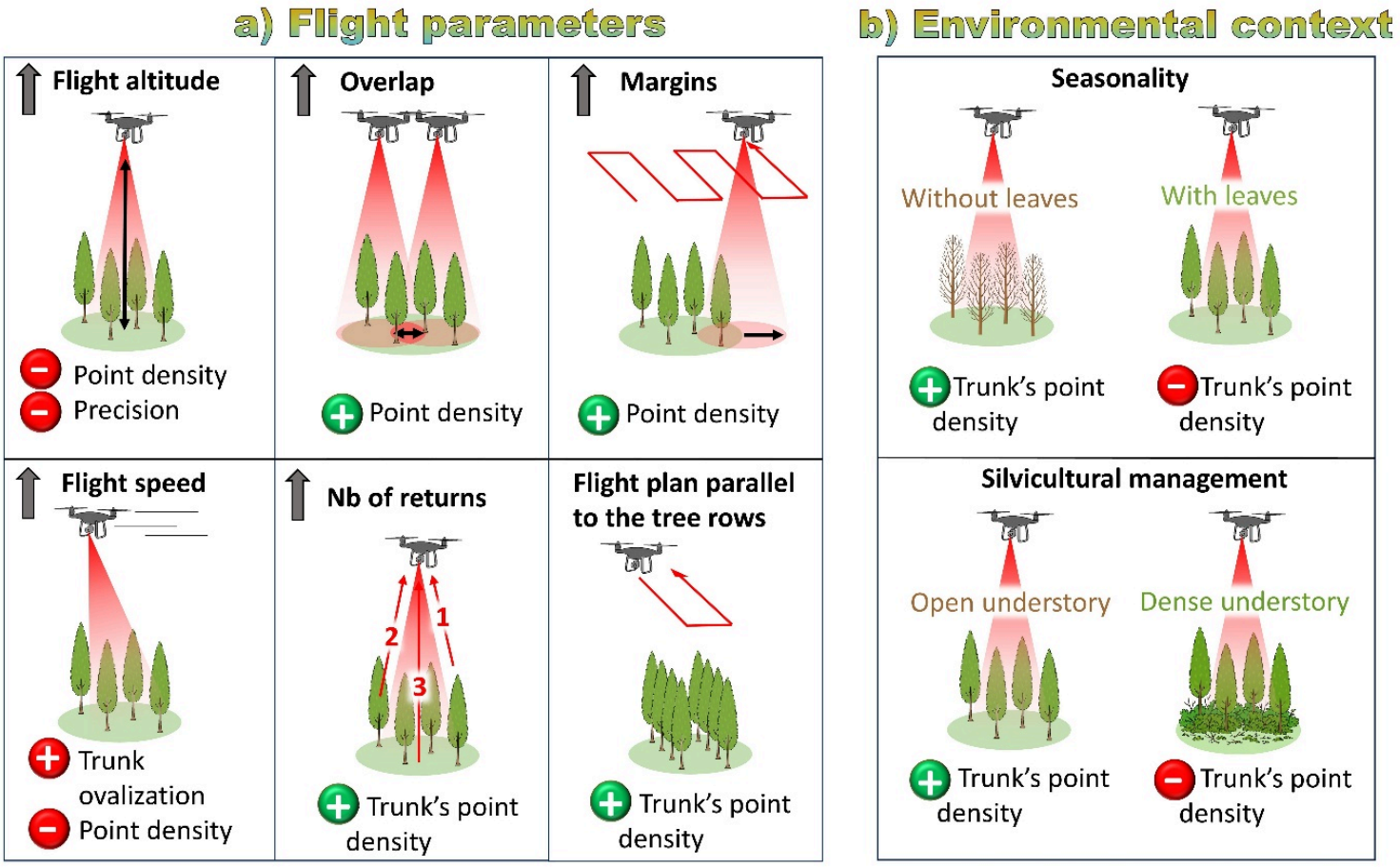


Figure 13

Impact of (a) flight parameters and (b) environmental context on the quality of UAV-acquired LiDAR point clouds. This figure is adapted from Eisenschink et al. (2025) and extended with findings from the present study.

Supplementary Files

This is a list of supplementary files associated with this preprint. Click to download.

- Appendices.docx